Author:
Kirkpatrick, Tom W M

Title:
Modelling Glacial Lake Outburst Flood Discharge in the Rio Huemules, Northern Patagonian Icefield

Modelling Glacial Lake Outburst Flood Discharge in the Rio Huemules, Northern Patagonian Icefield.

By

Thomas W. M. Kirkpatrick

School of Geographical Sciences

UNIVERSITY OF BRISTOL

JULY 2023

A dissertation submitted to the University of Bristol in accordance with the requirements for award of the degree of MASTER OF SCIENCE BY RESEARCH in the Faculty of Science.

Word count: 15 074

Abstract

The Northern Patagonian Icefield is one of the most rapidly changing ice masses on Earth and drains cold sediment laden fresh water into the critical aquatic zone of the Patagonian fjords. Glacial retreat and the growth of glacial lakes has caused repeated glacial lake outburst floods (GLOFs) in several rivers draining the icefield, but to date few studies have detailed flood hydrographs. This thesis presents a high resolution, multi-year discharge record for the Rio Huemules, a major river draining Steffen Glacier, third-largest glacier of the Northern Patagonian Icefield. To construct the discharge record, a rating was developed which combines fluorometric discharge gaugings at low stage and hydraulic modelling to estimate the stage—discharge relationship at peak flows. The rating was corroborated by comparison with discharge estimated using source lake volume and the Clague—Matthews relationship for subglacial pipe flow. Four GLOFs are documented, each with discharges exceeding 1000 m3/s. The largest event occurred in December 2016, reaching a peak discharge of 3432 m3/s ± 25% after an outburst flood from the Laguna de los Tempanos. As Steffen Glacier undergoes accelerating retreat, the water storage capacity of the Laguna de los Tempanos is diminishing, resulting in a decline in GLOF magnitude in the Rio Huemules. However, as retreat of the main glacier trunk progresses up valley, a roughly 0.2 km3 lake to the north of Laguna de los Tempanos may enter a GLOF phase in the near future, potentially leading to flood discharges exceeding 3000 m3/s. This rating contributes to risk management for families in the Lower Huemules valley and adds to studies on the catchment water balance for the Steffen Glacier system and regional biogeochemical cycles.

Dedication and Acknowledgements

Sincere thanks to Professor Jeffrey Neal, who began this project as my secondary supervisor but gave so much more than that title suggests. Your relentless good humour and wise advice are the foundation this thesis was written on. Thank you to Professor Jemma Wadham, who created this project and gave me the chance to work on it, who was a wonderful fieldwork partner and who gave me so much during the difficult days of the first Covid lockdown. Jemma, your energy and love for the icy parts of the world are an inspiration. I still can't believe I forgot that wrench. Finally, thank you to Dr Chris Yates, whose help in tracking down and wrangling together all the various scattered parts of the stage record was invaluable.

I would like to dedicate this thesis to my gramps, Eric Baker, who died before I even came to the University of Bristol, but who would have been fascinated by the mathematics underpinning this work and would have understood them far better than me.

Also, Lauren, I know you were hoping for me to write something more original than this, but I couldn't have finished this thesis without your support. I am very lucky. Next step: fieldwork together...?

Author's Declaration

I declare that the work in this dissertation was carried out in accordance with the requirements of the University's *Regulations and Code of Practice for Research Degree Programmes* and that it has not been submitted for any other academic award. Except where indicated by specific reference in the text, the work is the candidate's own work. Work done in collaboration with, or with the assistance of, others, is indicated as such. Any views expressed in the dissertation are those of the author.

SIGNED: Tom Kirkpatrick DATE: 20th July 2023

Table of Contents

List of Tables

List of Figures

1 Introduction

1.1 Glacial Lake Outburst Floods

Glacial lake outburst floods (GLOFs) are a natural hazard caused by the sudden release of water from glacial lakes, typically due to a breach in the ice or moraine dam that contains them. These floods can result in significant damage to infrastructure and can be catastrophic for downstream communities, as well as having an acute impact on local and regional ecology.

The term glacial lake outburst flood gained general acceptance during the 1980s but may be traced back to very early work in German by Michael Stotter (1846) and Eduard Richter (1892) who discuss *"ausbrüche des gletschers"* or outbursts of the glaciers and glacial lakes. In "Glacial Reservoirs and their Outbursts" (Rabot, 1905), Charles Rabot describes in detail pro-glacial, supra-, sub- and en-glacial lakes, as well as ice-dammed lakes which form when glaciers obstruct valleys and dam water within them. The sudden destructive power and widespread hazard of glacial lake outburst floods was well known by mountain people, and Rabot discusses historical accounts of outbursts as early as the 1590s in the Alps, as well as contemporary occurrences in glaciated mountain regions worldwide. By the 1950s much research was being done on the glacial lake floods of Iceland and the Icelandic term *"Jökulhlaup"* from *jökul* (glacier) and *hlaup* (literally to run or leap), became common. This thesis will use GLOF or jökulhlaup to describe the same phenomenon, depending on the choice of the literature being referenced.

Today research into GLOFs is a rapidly growing field which includes both theoretical modelling and empirical studies. Researchers have used advances in remote sensing and machine learning techniques to inventory and monitor glacial lakes and to develop models that can predict the likelihood and impact of GLOFs (Aggarwal et al., 2017a; Dabiri et al., 2021; Dai et al., 2022; Strozzi et al., 2012; Wangchuk et al., 2019, 2022). Additionally, field studies have provided valuable insights into the dynamics of GLOFs, including the factors

that contribute to the failure of glacial dams (Iribarren Anacona et al., 2018) and the behaviour of flood waves and debris entrainment (Jacquet et al., 2017; Osti and Egashira, 2009).

The complexity of GLOF susceptibility indicators and conditions leading to dam failure mean that there is no general mechanistic model for GLOFs, and global characterisation of GLOF processes often misses key regional differences (Emmer et al., 2022). However, global trends in GLOF occurrence are important to discuss. Increased glacial retreat caused by global climate change in the 20th century has caused the growth of thousands of glacial lakes with the potential for outburst floods. Shugar et al. (2020), show that between 1990 and 2018 the number of glacial lakes and their total surface area has increased by 53 and 51 percent respectively, with the largest lakes exhibiting the greatest relative areal increases. Most of these large lakes are in medium to high latitude glaciated regions such as Alaska, northern Canada, Scandinavia, Greenland and Patagonia. But whether this increase has resulted in more GLOFs is not settled science. The most comprehensive global GLOF inventory suggests that while the occurrence rate of GLOFs from moraine dammed pro glacial lakes has remained steady since the mid-20th Century, GLOFs from ice-dammed lakes have become more frequent, but the temporal and regional biases in long-term GLOF inventories are suggested to be significant. Between two and four out of five GLOFs may have gone unreported in the early to mid-20th century, and historical reporting is almost certainly biased towards densely populated mountain regions with long traditions of mountaineering and scientific research (Lützow et al., 2023; Veh et al., 2022).

It seems that GLOFs evident in the sparse early satellite record are potentially lucky exceptions available for researchers to study, while today's satellite constellations which allow revisit times of 12 days or less dramatically increase our chances of imaging GLOF events. Satellite data can be used to estimate the date, volume of water, type of dam failure and downstream inundation caused by a GLOF, but for detailed analysis of the flood direct measurements of the flow within the river channel are invaluable. Despite the increase in GLOF reporting, less than a quarter of GLOFs in the inventory include hydrograph data or detailed information on the downstream effects, and the Andes are particularly data poor,

with fewer than 15 percent of reported GLOFs including gauged or estimated values for peak discharge and flood volume (Lützow et al., 2023).

The mechanics of GLOFs are complex, involving processes such as ice or moraine dam failure, interaction with subglacial meltwater drainage, and the transport of large volumes of sediment and debris. Similarly, GLOF discharge is highly variable, depending on factors such as the size and depth of the glacial lake and the mode of failure of the ice or moraine dam. The same glacial lake may release outburst floods of hugely different volume depending on temporarily existing conditions that govern those factors. GLOFs typically result in sudden and extreme changes in river levels, making it challenging to predict and manage these events.

GLOF hazard is a function of the likelihood and potential magnitude of an event. Clearly GLOF hazard is a local metric, dependent on the specific conditions present at a point in time in a particular glacial system. The likelihood of an event depends on the interplay between multiple dynamic factors, including most importantly: lake dam stability; presence of potential meteorological or topographic triggers such as extreme precipitation events, landslides, avalanches or calving events; and lake volume. Lake volume largely controls the event magnitude, while also contributing temporal variability because GLOF likelihood will remain low for some time immediately following an event (Taylor et al., 2023). Studies on GLOF risk consider the hazard in tandem with complex natural and socio-economic factors which determine the potential for harm to human life, property or infrastructure. In many mountain areas settlements, agricultural land and transport and energy infrastructure are forced by valley terrain to occupy potential GLOF outflow paths, creating difficult problems for risk management (Anacona et al., 2015; Frey et al., 2016; Motschmann et al., 2020; Taylor et al., 2023).

The extreme river discharges involved during GLOF events induce significant scour, sediment transport and deposition throughout the glaciofluvial system, and further into marine environments where these lie close to the source of the GLOF. Where GLOFs tunnel subglacially, huge amounts of sediment can be transported from the bed of the glacier.

Further downstream the high velocity flows can erode the riverbed and banks, entraining large amounts of sediment both in suspension and as bedload. This can significantly alter fluvial morphology and destroy riparian habitat. As the flood energy decreases downstream, much of this sediment is deposited leading to the formation or enlargement of gravel and sand bars and deltaic fans.

In places like Greenland and Patagonia where glacially fed rivers discharge into fjords, the sediment laden freshwater from the GLOF forms a hypopycnal plume which floats on top of the denser ambient water body. Upon discharging into the fjord this plume spreads out at the water surface forming a distinct layer which can deposit sediment over large areas of the benthic environment and alter circulatory currents, light penetration and temperature which can affect the entire system of primary productivity (Piret et al., 2022; Syvitski, 1989; Zavala et al., 2021).

1.2 The Northern Patagonian Icefield

The modern day Northern and Southern Patagonian Icefields are remnants of a Pleistocene ice sheet that almost completely covered the Andes south of around 38 degrees during the last glacial maximum (Glasser et al., 2008). Now separated by the Baker Martinez channel, the Southern Patagonian Icefield, 12,232 km^2 and the Northern Patagonian Icefield, 3,675 km^2 are respectively the largest and second-largest continuous extra-polar ice masses in the southern hemisphere (Meier et al., 2018) and dominate the southern Andes cryosphere. The icefields are characterised by steep mountains and relatively low altitude accumulation areas which lie directly in the path of the South Pacific westerly wind belt. These moisture laden winds from the open ocean are forced upward by the terrain and deposit extreme amounts of precipitation on a steep gradient from west to east across the orogen. Coupled with the relatively mild temperatures – the NPI extends to - 47.5 °S – and outlet glaciers terminating near or at sea level, this leads to an extremely dynamic glacial system (Warren and Sugden, 1993).

Due to its remote location and challenging terrain, the Northern Patagonian Icefield has remained relatively understudied compared to other regions with significant glacial activity. However, recent advances in remote sensing and growing capacity for field research have shown it is one of the most rapidly changing temperate ice masses in the world, experiencing increasing rates of mass loss over the last 50 years (Bravo et al., 2021; Davies and Glasser, 2012; Dussaillant et al., 2018; Meier et al., 2018; Rivera et al., 2007). Rising temperatures have led to increased melting and a consequent retreat of most glaciers, resulting in the formation and expansion of glacial lakes (Dussaillant et al., 2010). As these lakes grow in size, they exert increasing pressure on their ice or moraine dams, raising the likelihood of dam failure and GLOFs, as well as contributing positive feedbacks which hasten glacial mass loss (Bravo et al., 2021).

The Patagonian Icefields account for 90 percent of the fastest thinning ice found in the Southern Hemisphere, and have the largest contribution to sea level rise relative to their area of all ice masses globally (Jakob and Gourmelen, 2023; Rignot et al., 2003). This contribution is delivered in two ways: directly through frontal calving of tidewater glaciers such as Jorge Montt glacier of the SPI, and by increased meltwater from thinning land and lake terminating glaciers like Steffen and Collonia.

1.3 Steffen Glacier

Steffen Glacier is the third largest glacier of the Northern Patagonian Icefield and is wasting at a rate of up to -6 m surface elevation change per year (Jaber et al., 2014), a rate which may be accelerating (Abdel Jaber et al., 2019). It flows roughly south off the icefield, terminating in a large proglacial lake which is drained by the lower Huemules River. The 18 kilometre long channel of the lower Huemules River exits the proglacial lake flowing east, before bending southwards through a steep-sided valley and then gravel and sand bars to its delta at the head of Steffen Fjord, part of the Baker Martinez channel system – figure 1.1.

Four ice dammed lakes also drain into the Huemules river. Laguna de los Tempanos; GL1, an un-named glacial lake similar in size and orientation to Laguna de los Tempanos; GL2, which is dammed far up the main body of Steffen Glacier near the confluence of its two tributary arms; and GL3, which is dammed by the rapidly retreating snout of glacier HPN4, a land terminating spur of Steffen Glacier.

All four ice-dammed lakes in the Steffen system have been suggested to release outburst floods, with Laguna de los Tempanos releasing the largest magnitude events. In 2016 a field team from the University of Bristol fixed Onset Hobo and Keller CTD pressure transducers in the Lower Huemules to gather data on the flow regime. Preliminary analysis of the stage record identified a GLOF in late March 2017 and estimated discharge for that event at 2,600 m^3/s (Aniya et al., 2020), but how this discharge was calculated is unclear and otherwise GLOFs in the Steffen Glacier system have only been identified using satellite and aerial survey imagery. To date, there is no physically based model for describing the stage discharge relationship in the Huemules River.

Defining the stage discharge relationship in the Lower Huemules river is essential for beginning to understand the hydrological balance in the Steffen Glacier catchment, and therefore a significant fraction of the entire Northern Patagonian Icefield. This knowledge will inform our study of terrestrial freshwater delivery to the region's delicate fjord ecosystems, which are a valuable natural laboratory for contemporary and palaeo glacio-marine sedimentology (Piret et al., 2021; Van Wyk de Vries et al., 2022; Vandekerkhove et al., 2020a).

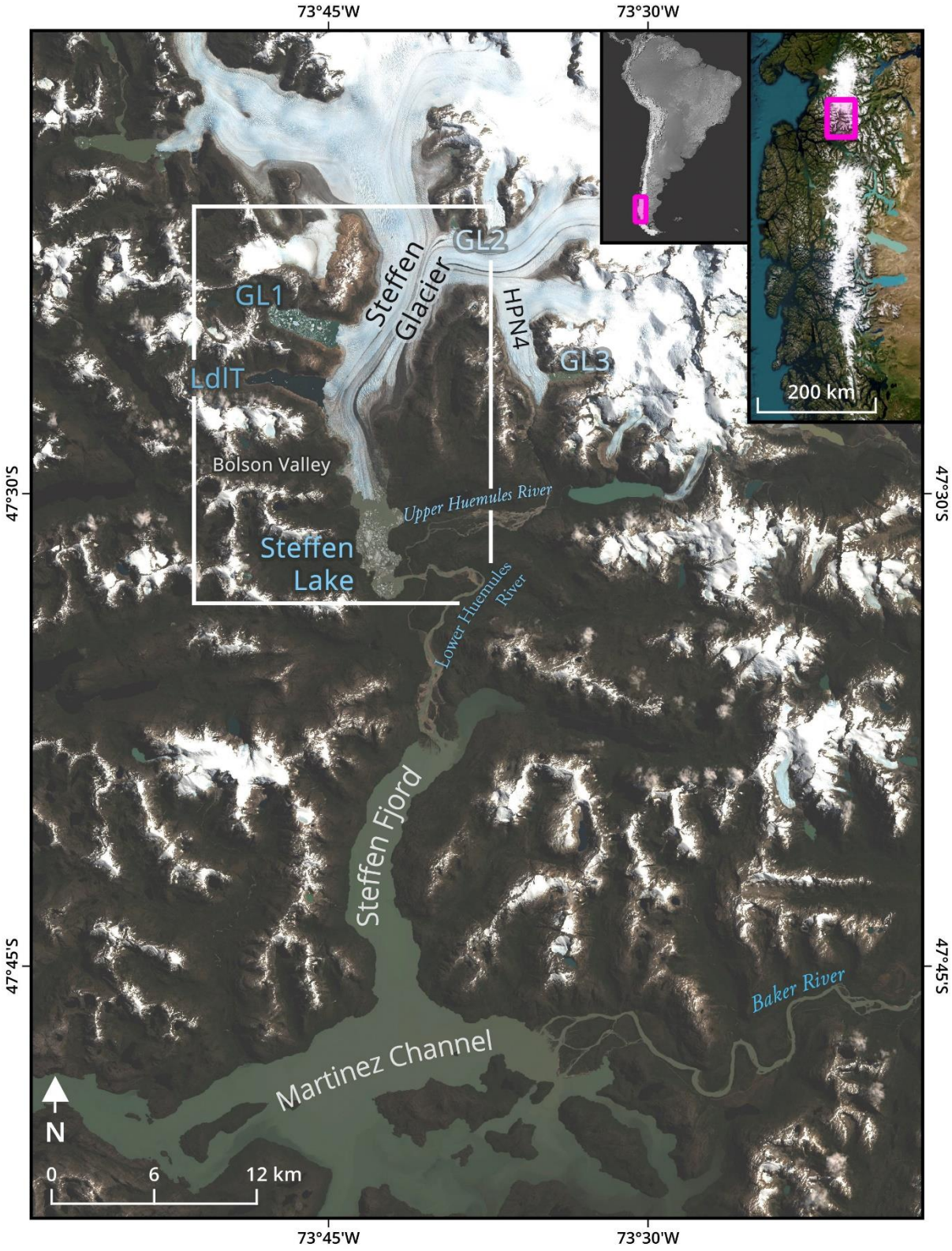

Figure 1.1: Map of the Steffen Glacier system and the Martinez Channel (Modified Landsat 8 image courtesy of the U.S. Geological Survey processed by Sentinel Hub).

1.4 Research questions

- Can basic site knowledge gained during a field visit be combined with remote sensing and hydraulic modelling to produce a realistic rating and capture high magnitude/low frequency flow events in the Lower Huemules river?
- Can the GLOF hydrographs tell us anything about the mode of failure and drainage pathway?
- How does the discharge record from the Lower Huemules compare to other rivers which drain the Patagonian Icefields?

1.5 Summary

Glacial lake outburst floods are a major natural hazard present in all glaciated mountain environments and pose significant risk to human life, livelihood and infrastructure, as well as causing lasting geomorphic and ecological change. The southern tip of South America is dominated by the Northern and Southern Patagonian Icefields and as climate change leads to widespread glacier retreat, the impact on GLOF frequency and magnitude remains debated. In contrast to mountain regions in Europe and North America, hydrological data for GLOFs in the Andes is scarce. This thesis aims to create a hydrological record based on stage data from a major river draining the Northern Patagonian Icefield, which can be used to describe past GLOFs from the Steffen Glacier system and inform the potential magnitude of future hazards.

2 Literature review

This literature review introduces the history of glacial lake outburst floods in the Patagonian cryosphere before discussing research into the triggers, drainage mechanisms and pathways, and hydrograph characteristics of GLOFs. Sections 2.3 and 2.4 present the physical, ecological and socio-economic impacts of GLOFs in the Southern Andes, and section 2.5 discusses how climate change may shape future GLOF risk in Patagonia.

2.1 Glaciers and glacial lakes in Patagonia

Glacial lakes and their outburst floods are perennial feature of glaciated regions today and in the past, and clues of their magnitude and frequency can tell us about the processes of the cryosphere environment in which they occurred (E.g., Carrivick and Tweed, 2013; Frey, 2017; Jansson, 2003; Murton and Murton, 2012).

The six largest outburst floods in the Quaternary geological record all resulted from the failure of ice-dams formed as advancing ice sheets blocked existing major river valleys, or through the genesis of ice-marginal lakes – possibly during periods of ice-sheet instability (O'Connor and Costa, 2004). By far the largest of these events – the Late Pleistocene Kuray megaflood in Altai, modern day Russia, and the Missoula megaflood in the northwestern USA are supposed to have generated peak discharges of 17 million and 18 million m^3/s respectively (Baker et al., 1993; O'Connor and Baker, 1992), and are among the largest magnitude sediment transport events known (Korup, 2012). Such enormous discharges result in areas with high relief and thick ice sheets impounding vast lakes because outburst discharge increases exponentially with breach depth. The ice dams whose failure caused the Kuray and Missoula outburst floods would have been around 600 – 1,000 m high (Baker et al., 1993; O'Connor and Baker, 1992; O'Connor and Costa, 2004).

Evidence of palaeo-megafloods has also been found in the Southern Hemisphere, where the former Patagonian Icesheet covered many times the area of the modern-day icefields and stretched from 38°S to 56°S (Glasser et al., 2008). Palaeosol deposits dated to the Last Glacial Interglacial Transition around 12 – 10 kya indicate a period of very high magnitude floods with modelled peak discharges reaching approximately 110,000 m^3/s (Benito and Thorndycraft, 2020). Further evidence suggests a minimum of 86 palaeo GLOFs exceeding 3,500 m^3/s over the last 10,000 years in the Baker River valley – Chile's largest river by mean annual discharge (Benito et al., 2021; Dussaillant J. et al., 2012). Periods of increased flood frequency occurred around 4.3 kya and again between 2.57 and 2.17 kya. The first of these coincided with the end of the mid-Holocene neoglacial as glacial instability caused repeated ice-dam collapse, while the later period has been linked to lower temperatures and increased precipitation causing glacial advance. The same analysis indicates that GLOF magnitude generally declined through the Holocene as glaciers thinned and retreated, thereby impounding smaller and shallower lakes (Benito et al., 2021; Vandekerkhove et al., 2020b).

The most recent neoglaciation in Patagonia occurred between the 17th and 19th centuries, a global period of cooling known as the Little Ice Age which caused glacial advance worldwide (Aniya, 2013; Bräuning, 2006; Espizua and Pitte, 2009; Kjær et al., 2022; Koch and Kilian, 2005; Rowan, 2017). Since then, as Patagonian glaciers have retreated to their current positions, studies have shown an increase in the area and volume of Patagonian glacial lakes (Loriaux and Casassa, 2013; Wilson et al., 2018). This is mirrored in the Peruvian Cordillera Blanca (Emmer et al., 2020), and indeed globally (Aggarwal et al., 2017b; Shugar et al., 2020).

Accurately measuring lake volume requires bathymetric surveys that are costly and dangerous to perform in remote and hazardous mountain environments, but the threat of damaging floods from remote glacial lakes has encouraged the development of indirect methods for estimating lake volume, for example from satellite derived water surface area measurements (Cook and Quincey, 2015; Huggel et al., 2002; Loriaux and Casassa, 2013). The relationship presented by Loriaux and Casassa (2013) for the Northern Patagonian Icefield adapts existing surface area to volume relationships by adding region specific data on known lake volumes. They suggest a surface area-based error of ±5 percent, based on ±1

pixel uncertainty in lake surface delineation. This equates to roughly a ±6.5 percent error in calculated lake volume using their method. However, Cook and Quincey (2015) note that even glacial lakes within regions can vary significantly in their surface area to volume relationship, with error over 100 percent in some cases, suggesting such calculations should be used with caution. Water surface area measurements can be semi-automated by employing band ratios or normalised difference water index (NDWI) from multispectral satellite imagery (Li and Sheng, 2012; Wang et al., 2020), or backscatter thresholding of synthetic aperture radar (SAR) imagery (Strozzi et al., 2012; Zhang et al., 2019), but the topography of the NPI complicates use of automated methods. Dense brash ice and icebergs often crowd the lake surfaces making automated waterbody delineation challenging where they abut wet glaciers, and the steep valley sides interfere with both optical and SAR imagery by casting shadows over the water surface which make accurate identification of the shorelines difficult.

In their review of terrestrial water storage in the glacial lakes of the Northern Patagonian Icefield, Loriaux and Casassa (2013) found that manual delineation of the water surface proved more accurate. Over a study period from 1945 to 2011 and using imagery sources ranging from oblique analogue aerial reconnaissance photographs to contemporary multispectral satellite imagery, they found that the total glacial lake surface area had increased by 66.0 km^2, corresponding to a volume increase of 4.8 km^3 over the same period, with most of this increase occurring after 1987 in tandem with the increased rate of glacial mass loss since the 1990's (Aniya and Casassa, 1998; Davies and Glasser, 2012). Most of this increase occurred in the moraine-dammed pro-glacial lakes of Steffen and San Quintin glaciers, which increased by 18.0 km^2 and 9.0 km^2 respectively due to glacial front retreat, and between them accounted for 31.7 percent of the measured glacial lake volume in 2011. In contrast, the area and volume of ice-dammed glacial lakes decreased slightly between 1945 and 1976, with the authors finding no trend thereafter (Loriaux and Casassa, 2013).

The mechanisms responsible for this difference appear reasonably simple. The moraines which now hold back the pro-glacial lakes of the Northern Patagonian Icefield were built during the Little Ice Age glacial maxima and since then their elevation has remained

relatively stable (Glasser et al., 2008). In contrast the ice dams which control the level of Laguna de los Tempanos and other marginal lakes are constantly shrinking with glacial margin retreat, and simultaneously the drainage path under the glacial tongue is growing shorter and shallower (Davies and Glasser, 2012). So, for moraine dammed lakes of the NPI, the ultimate control on lake surface elevation – the height of the terminal moraine, has remained stable while the area of the lakes has increased due to glacial front retreat. But for ice-dammed lakes the limits on lake surface elevation have been reducing at the same time as the hydrostatic pressure required to force a breach and GLOF, has been reducing. In the Steffen glacier system this results in perpendicular ice-marginal valleys entering a sequential GLOF cycle governed by glacial retreat from south to north, most easily seen in the histories of Laguna El Bolsón, Laguna de los Tempanos and Glacier Lake 1 (Aniya et al., 2020).

Aniya et al. (2020), inspected 150 optical images of Steffen glacier and Laguna de los Tempanos to determine the GLOF history of the lake, also describing GLOFs from Laguna El Bolsón and Glacier Lake 1 (GL1) — see map in figure 1.1. The images included both oblique and vertical aerial survey imagery, but the majority – 132 – were Landsat images from the MSS, TM, ETM and OLI sensors. Occasionally long and irregular time periods between images make GLOF events difficult to determine with certainty, and their precise timing is even less sure, but low lake water level combined with icebergs stranded on the dry lakebed was defined as the strongest indication that a GLOF had occurred shortly before the image acquisition. As well as these 'certain GLOFs' the authors inferred some GLOFs had occurred from a number of less obvious signs in a holistic interpretation of sequential images, including crowding of icebergs at the glacier margin, and smaller but still visible fluctuations in lake level. Overall, 16 certain GLOFs are described for Laguna de los Tempanos, with a further 3 inferred as probable. The authors do not describe the GLOF of December 2016, because there are no cloud free images available of this event, although it is visible in radar imagery from the European Space Agency's Sentinel 1 satellite.

Laguna El Bolsón was suggested to have released GLOFs six (possibly eight) times, with the most recent being in 2008, after which it has become connected to Steffen Lake as the glacier tongue has retreated closer to the mouth of valley it once dammed. In the no name lake

north of Laguna de los Tempanos, they register nine GLOFs, some potentially very small, with only one of those occurring since the lower, main basin of the lake has filled.

Discharge from glaciated rivers in the Northern Patagonian Icefield is not well quantified at present due to the lack of direct gauging stations. Measurements of discharge for the Nef and Colonia rivers have been made by differencing discharge measured up and downstream of their confluence with the Baker River, and these show a distinct seasonality with the highest flows generated by melt in December and January (Dussaillant J. et al., 2012). Repeated outburst floods from the approximately 215×10^6 m^3 (0.22 km^3) Cachet 2 lake which drained into the Baker via the Colonia River were captured on the Baker—Colonia confluence gauges and showed a steep rising limb followed by a more gentle recession, and maximum discharge of 1500—2600 m^3/s with the Baker's base flow subtracted (Jacquet et al., 2017). These peak GLOF discharges represent a 2—4 -fold increase in discharge over mean peak annual discharge in the Colonia River, although the 40 km distance between the gauging station and the source lake results in significant attenuation of the flood signal. Direct gauging of stage in the source lake indicated a hydrograph with a gradual rising limb and an abrupt recession, with median peak discharge from the source lake estimated at 4300 m^3/s, but maximum estimates exceeded 10 000 m^3/s (Jacquet et al., 2017).

2.2 Hydrodynamics of ice-dammed lake outburst floods

Early qualitative studies on outburst floods from the glacial lakes of Iceland's Vatnajökull suggested the ice dams were breached as hydrostatic pressure built up sufficiently to allow floatation of the glacial ice and subsequent subglacial drainage by sheet flow (Thorarinsson, 1939). Using this hypothesis Thorarinsson showed how outburst floods from ice-dammed lakes could be used as indicators of glacier oscillation between periods of thinning and retreat, and periods of advance. Glen (1954) proposed a refinement of the subglacial drainage mechanism by suggesting that once hydrostatic pressure has exceeded the ice pressure of the glacier at the deepest point of the ice dam the water pressure forces a subglacial drainage tunnel by plastic deformation of the ice. This better explains the total

emptying of the glacial lakes mentioned by Thorarinsson, and fits with the more-or-less exponential rising limb of observed GLOF hydrographs, but Liestøl (1956) recognised that subglacial tunnel enlargement during GLOFs was more likely caused by melting – first due to the small relative temperature difference between the glacial lake water and the ice dam, and subsequently increasing due to the frictional heating of water flowing through the tunnel.

In a review of data from the outburst floods of six different ice-dammed lakes, Clague and Matthews (1973) showed that peak discharge during ice-dammed lake outburst floods was roughly proportional to the total volume of water released during the flood raised to the power of two-thirds, and subsequent investigation has shown this 2/3 exponent to be consistent for subglacially draining lakes (Ng and Björnsson, 2003; Walder and Costa, 1996). Over the following decade, detailed studies focussing especially on the jökulhlaups from the Grímsvötn subglacial lake of Iceland's Vatnajökul icecap, defined the physics that govern turbulent water flow through subglacial conduits and the dynamic balance in which the tunnel is simultaneously enlarged by frictional melting, and constricted by the overburdening ice pressure (Nye, 1976; Röthlisberger, 1972). Clarke (1982) and Spring and Hutter (1981) expanded on Nye's model and the Clague–Matthews formula by introducing reservoir geometry as an important input factor governing pressure head at the entrance to the breach, and showed that "creep closure" — the tunnel constriction caused by overburdening ice pressure — was insignificant compared to melting caused by relatively warm flood waters, but became the dominant force as water pressure in the tunnel fell towards the end of the flood. These studies had focussed on subglacial tunnel drainage from subglacial and ice-marginal ice-dammed lakes, but further work expanded the basic equations to describe how the flood hydrograph is affected by the mode of lake drainage. Breach type floods – where the outburst occurs due to mechanical failure of part of the ice dam – were shown to have a more abrupt onset and shorter overall duration than tunnel-drained floods, and the relationship between total flood volume and peak discharge was similar to that seen in the failure of earth constructed dams (Walder and Costa, 1996). These types of floods were more typically seen in glacial lakes formed by tributary glacier advance damming water in a trunk valley, while tunnel drainage floods occurred where ice-marginal

lakes formed due to glacial retreat leading to tributary glaciers collapsing earlier than the main glacier body, or, as in the case of Grímsvötn, due to subglacial lakes formed by geothermal action under ice caps (Walder and Costa, 1996).

Recent field studies have explored englacial drainage systems in a diverse range of glacial systems and found that channels can form as meltwater enlarges existing fracture lines and nascent crevasses in the ice – a process known as 'hydrofracturing' (Benn et al., 2009; Gulley et al., 2009). Crevasses do not typically reach deep down into a glacier because the compressive force of overburdening ice pressure overcomes any tensile stresses acting to fracture the ice, but where crevasses are filled with water this can compensate for the overburden pressure and lead to deep crevasse propagation (van der Veen, 1998).

Many of the previous studies exclude the role of sediments in subglacial drainage mechanisms (Clarke, 1982; Nye, 1976; Spring and Hutter, 1981; Walder and Costa, 1996) or mention it as an unknown that requires further research (Röthlisberger, 1972), but sediments, especially subglacial sediments, play a significant role in subglacial outburst flood drainage in a number of ways. To achieve a good fit between his model and the actual hydrographs from Grímsvötn jökulhlaups, Nye used a larger value for the Manning's n roughness co-efficient than would be expected for an ice-walled tunnel (Clarke, 2003), but by imagining a broader, lower ceilinged conduit and taking into account excavation of subglacial sediments, Fowler and Ng (1996) were able to more closely recreate the rising limb of the Grímsvötn hydrograph. Even relatively small glacial lake outburst floods can mobilise huge amounts of sediment. In 1968 a GLOF from a periglacial lake of Grubengletscher in the Swiss Valais released 170 000 m^3 of water with a peak discharge of just 10 m^3/s, but eroded around 400 000 m^3 of debris from Holocene and late-glacial moraines down valley (Haeberli et al., 2001).

As well as excavation of sediments from subglacial till, deposition also occurs in sub- and englacial tunnels, and infilling can result in conduit closure during the end-stages of a glacial lake outburst (Burke et al., 2012). These sedimentary deposits, called eskers, are sinuous ridgelines of sand and gravel sometimes tens of kilometres long, and are found in

post-glacial environments around the world (e.g., Banerjee and McDonald, 1975; Boulton et al., 2009).

2.3 Hydrological and geomorphic consequences of GLOFs in Patagonia

As previously discussed, sediment dynamics during glacial lake outburst floods are a key factor in the mechanics of drainage, as well as having large geomorphologic and ecological impacts along the whole flood route. Sediment can be mobilised from the source lakebed; subglacial till during tunnel formation or sheet flow; and glacial riverbeds and banks as the flood propagates downstream. Similarly, sediment can be deposited along the flood path leading to pockets of sediment blocking sub- and englacial conduits and cavities; deposition in proglacial lakes, glacial rivers and their deltas; and benthic environments in fjords and continental shelves. High magnitude GLOF events can cause long-lasting changes to these downstream systems. Reconstruction of a mid-20th Century GLOF from the Lucía Glacier's proglacial lake and analysis of sediment cores show the event deposited a 6 cm thick layer of turbidite at the head of the Baker Channel and caused avulsion of the Pascua river and its submarine channel (Piret et al., 2022).

One of the most accessible, and so richly studied, glacial lake and river systems of the Northern Patagonian Icefield begins at the Cachet and Colonia glaciers which flow west off the icefield and feed into the Baker River via Lago Colonia, and the Rio Colonia (a tributary of the Baker). Between 2008 and 2017, 21 episodic GLOFs drained from Lago Cachet Dos either through or under the tongue of the Colonia Glacier, into Lago Colonia and then down the Rio Colonia into the Baker River, where discharges between 2500 and 3600 m^3/s were measured and sediment scour and deposition caused significant change to the braid plain (Jacquet et al., 2017).

When sediment falls through the water column and settles on lake and seabeds it creates distinct layers called varves which record the annual hydrological cycle and also high magnitude depositional events under the right conditions (Amann et al., 2022; O'Sullivan,

1983; Zolitschka et al., 2015). Many proglacial lakes are difficult to access and dangerous due to the risk of iceberg calving, but the huge proglacial lakes left on the eastern margin of the Patagonian Icefields by the retreat of the Pleistocene icesheet provide an ideal venue for limnological studies. Analysis of varved sediment cores from Lago Plomo east of the North Patagonian Icefield, and Lago Argentino to the east of the South Patagonian Icefield show interannual and multidecadal variability in winter precipitation in western Patagonia (Elbert et al., 2012) and seasonal differences in lake thermal stratification (Van Wyk de Vries et al., 2022).

2.4 Ecological and socioeconomic implications

Fjord ecosystems are particularly affected by terrestrial freshwater, sediment and organic matter inputs because their often complex, maze-like submarine topography effectively elongates the transition zone between land and open ocean (Bianchi et al., 2020). The huge twin fjords of the Baker and Martinez channels divide the North and South Patagonian Icefields and receive freshwater input from both ice masses. The Baker River, Chile's largest river by mean annual discharge, enters the eastern end of the Martinez Channel at Caleta Tortel, a small community of fishers and tourist operators. The Baker River drains from both sides of the Andes watershed south of 20°S and receives sediment laden glacial meltwater from the Soler, Nef, Colonia and Pared Norte glaciers which flow off the western edge of the North Patagonian Icefield and drain into the Baker via tributary rivers. To the south, the Baker Channel receives glacial melt directly from the tidewater terminating Jorge Montt glacier and from the western margin of the South Patagonian Icefield via the Pascua River – figure 2.1.

Freshwater discharge into fjords typically results in a distinct stratification of the water column, with colder estuarine discharge floating on top of the denser saline oceanic water and reducing the vertical mixing of organic matter from the ocean. This stratification is intensified in the summer months by increased discharge from glacial meltwater but the sudden, high magnitude influx due to GLOFs can deepen the pycnocline and deliver

sediment deeper into the fjord, increasing turbidity and decreasing light penetration which can reduce primary phytoplankton production (Meerhoff et al., 2019, 2013).

Marshall et al. (2021) showed how seasonal differences in delivery of dissolved organic matter (DOM) and dissolved organic carbon (DOC) to Steffen Fjord and the Baker—Martinez channel are driven by glacial melt inputs. The Baker and Pascua rivers dominate with respectively around 50% and 38% of the freshwater and organic carbon influx, while the Huemules contributes around 6% of the freshwater and 2% of the organic carbon, though the authors note that discharge in the Huemules is not yet well quantified.

The Huemules River supports a small number of settlers who ranch horses on the outwash plain near Steffen Fjord and on the floodplain of the Upper Huemules. It is also important habitat for the endangered huemul deer (Povilitis, 1986). While the settler families' houses are not directly in the outflow path of floods, their long familiarity with extreme discharge events in the Huemules River may put them at greater risk when source lakes transition into a GLOF cycle.

In his theory of heuristic traps in recreational avalanche accidents, McCammon (2002) shows how familiarity with a hazard in a particular area can lead to people trusting simple rules of thumb that may not accurately portray their level of risk. In the case of the GLOFs in the Huemules River, source lake GLOF cycles appear to occur over two or more decades, potentially resulting in people 'getting used to' the frequency and magnitude of events, or more pertinently, noticing that frequency and magnitude has declined over recent years and assuming that trend will continue. Because GLOFs are episodic and a lake entering a GLOF cycle has the potential to cause much larger events than a lake exiting its cycle, a multi-year period of low magnitude, or no GLOFs at all has the potential to encourage behavioural changes that increase individual risk. This highlights the importance of gaining a better, more formalised understanding of GLOF cycles, and where possible communicating expected GLOF cycle transitions and magnitude to at risk groups.

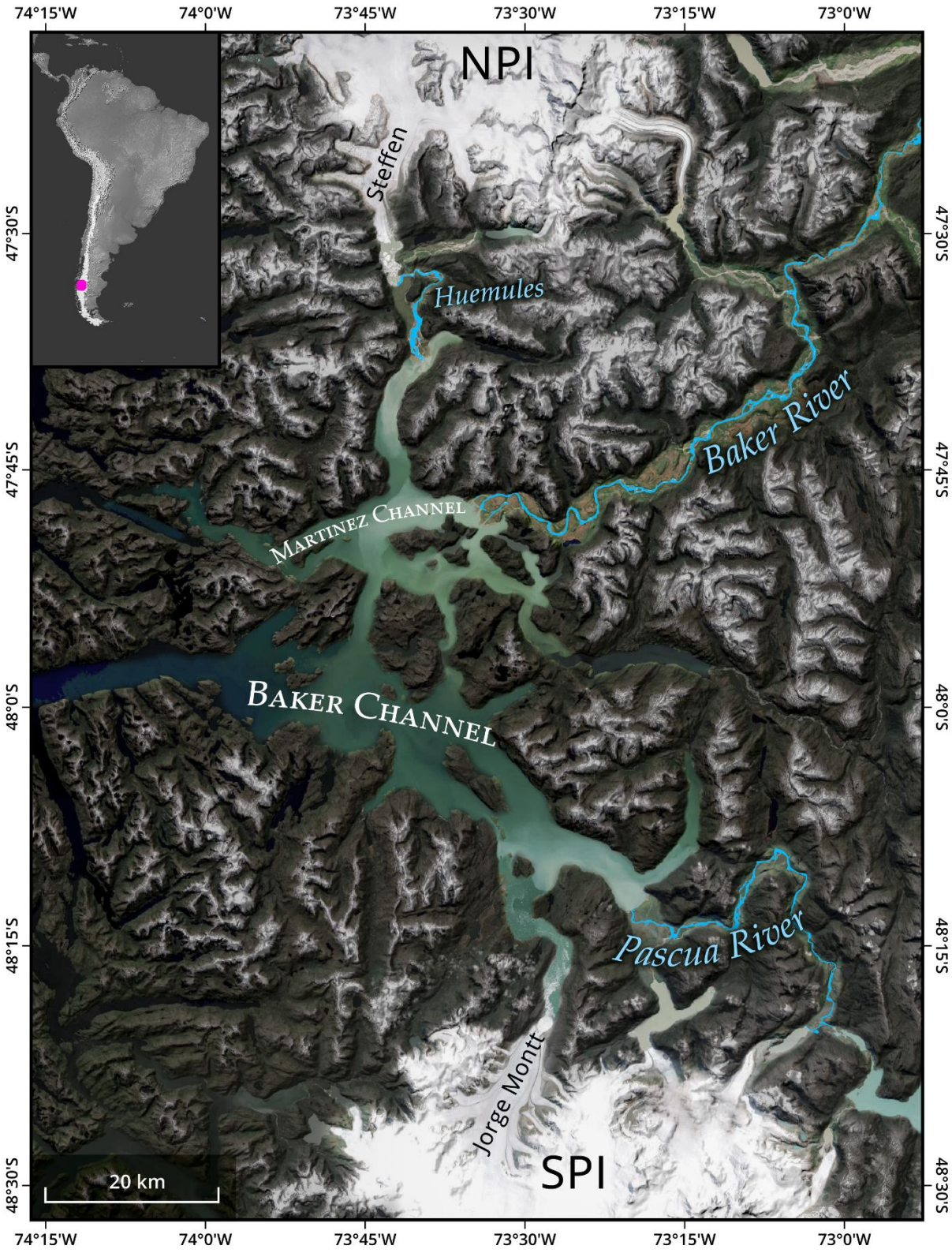

Figure 2.1: Landsat 8 image courtesy of the U.S. Geological Survey processed by Sentinel Hub. Image modified to highlight the Baker—Martinez channels with the Northern Patagonian Icefield (NPI) and Southern Patagonian Icefields (SPI).

2.5 Climate change and future GLOF hazard in Patagonia

The retreat of Patagonian glaciers since the Little Ice-Age is well documented by sedimentary and geomorphological studies, satellite altimetry, gravimetry and mass balance studies (Abdel Jaber et al., 2019; Davies and Glasser, 2012; Foresta et al., 2018; Jaber et al., 2014; Pereira et al., 2021) and is suggested to have an outsized impact on sea level rise relative to the size of other major ice masses (Richter et al., 2019; Rignot et al., 2003). Mass loss from the Patagonian Icefields alone is estimated to account for 16 ± 4% of the quantified sea level rise attributed to the melting of mountain glaciers worldwide (Hock et al., 2019). Under future climate projections the Northern Patagonian Icefield will remain in a surface mass balance deficit well into the middle of the century, and positive feedback processes such as growth of glacial lakes may accelerate this trend (Bravo et al., 2021).

Despite this, physically based studies of glacial hydrology in the Patagonian Andes are rare and a significant knowledge gap exists at the individual glacier and catchment scale (Pellicciotti et al., 2014). Refining our ratings for the stage—discharge relationship in gauged rivers fed by Patagonian glaciers can greatly improve glacial mass balance studies by helping to quantify the hydrological balance of the catchment (Van Wyk de Vries et al., 2023).

How this retreat translates to future GLOF risk across the region is uncertain, although for the Steffen Glacier system the work of Aniya et al. (2020) provides a very strong indication that as the front of Steffen Glacier continues to retreat, the Laguna de los Tempanos will eventually transition out of its GLOF phase just as Laguna el Bolson did at some point during the 1990s. It is also likely that lake GL1, which is similar in size and orientation to the Laguna de los Tempanos, will enter a phase of full drainage outburst floods at some point in the coming years.

2.6 Summary of literature review

In summary, the Northern Patagonian Icefield is a globally important component of the South American cryosphere with an outsized contribution to sea level rise compared to other mountain glacier regions. Steffen Glacier, the 3rd largest glacier of the NPI, is losing mass at an accelerating rate which has contributed to the growth of several glacial lakes. Glacial lake outburst floods are a major natural hazard found in glaciated regions, with significant environmental impact and risks to human life, and numerous GLOFs have been recorded in the Steffen system in the last 40 or so years. Defining stage—discharge relationships for glacial rivers is an essential part in understanding catchment scale water balance, and sediment transport but physically oriented studies of glacial hydrology in the Patagonian Icefields are rare and represent an important knowledge gap to fill.

3 Methods

Figure 3.1 is a visual representation of the methods used in this work. Hobo water pressure data (3.1.1) and inferred stage (3.1.2) were cleaned to produce the stage record. To estimate discharge, ratings were developed by estimating a compound channel cross-section (3.2.3), slope (3.2.4) and bed roughness (3.2.5) to calibrate a model using Manning's equation (3.2.8), and output an envelope rating for the Lower Huemules (3.3). The rating was tested at high stage by comparison with estimates of GLOF Qmax provided by source lake volume and the Clague—Matthews relationship (3.4).

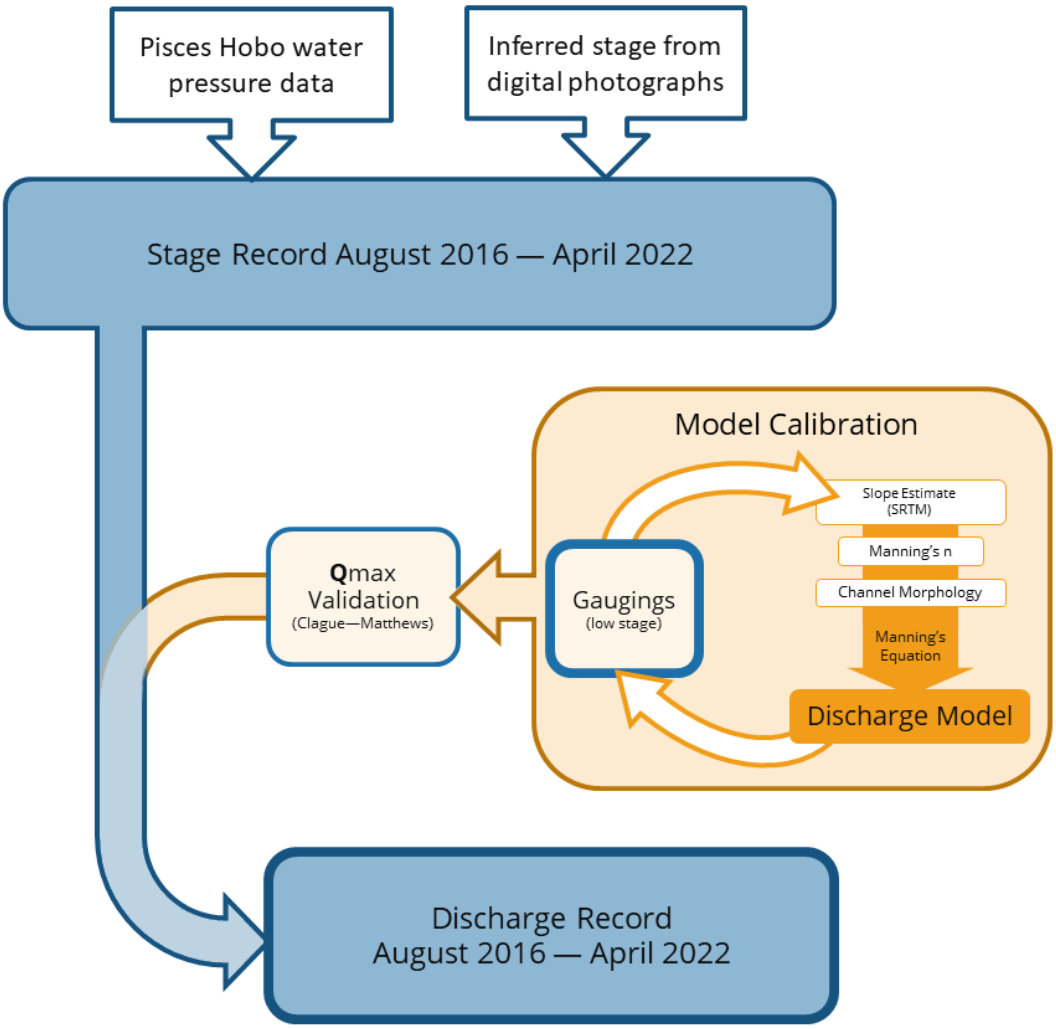

Figure 3.1: Method diagram.

3.1 Water level data

3.1.1 Pressure sensors

In August 2016, a University of Bristol field team fixed Onset Hobo pressure transducers to a bedrock outcrop in the Huemules River, roughly 1.7km downstream of its outflow from Steffen Lake, and shortly before the river enters a confined bedrock reach. One sensor measuring water pressure was bolted to the side of the outcrop in a backwater pool at Lat: --47.54219°, Long: -73.67304°, and an air pressure sensor was fixed to a steel scaffold on top of the outcrop that also supports a basic weather station for the DGA (Dirección General de Aguas). The water pressure sensor is approximately 30 cm above the sediment bed of the side channel and is frequently exposed to air during low water periods in the Austral winter. During these times the transducer records zero water depth, but flow remains in the main channel which is between 30 and 60 m wide in the bedrock reach downstream of the HOBO site – figure 3.2.

Figure 3.2: Location of the HOBO pressure transducer in a backwater pool (photo: Jemma Wadham).

These sensors recorded water pressure, atmospheric pressure and temperature data at 15 minute intervals since their installation in August 2016, except for a roughly year-long period between the 22nd November 2017 and the 1st November 2018, when the water pressure sensor failed. In October 2019 the sensors were set to a 1 hour recording interval to increase the length of time between field visits to download data. Water pressure readings in kPa are converted to sensor depth in metres by correcting for atmospheric pressure automatically in Hoboware Pro software.

3.1.2 Time-lapse photography

The failure of the water pressure transducer in November 2017 encouraged an attempt to infer water level from another source of data.

In June 2017 a SpyPoint SOLAR camera had been attached to the DGA scaffold and set to record images of the Lower Huemules River at 30 minute intervals. The camera faces upstream roughly south-southwest, towards a steep bedrock bank just to the south of the outcrop. Although the camera was not installed specifically with the intention of providing back-up water level data, this bedrock bank provides a fixed, nearly vertical feature against which it is possible to roughly infer water level. The camera records metadata for each image including exposure length and f stop, as well as time and date.

To estimate water level from the "unknown level images" during the period of missing HOBO data, a training set of "known level" images that were acquired while the pressure sensor was recording data was chosen. The pool of suitable images from which to draw this sample was small, because most images were acquired at times when the light was poor, or fog or rain reduced the clarity of the image and made it impossible to delineate the water level against the bedrock bank. Another difficulty was that most of the images acquired during periods of high water were mis-aligned after the camera was knocked out of position. In total, 9 images were selected as the training set. Each image was matched to the closest available water level measurement from the HOBO transducer, so that the images were associated with a water level reading acquired within 15 minutes of the image

acquisition. The training set was loaded into QGIS and a vector layer produced by tracing the water level in each image. The traced water levels represented a range of sensor depth readings from 0.039m to 3.255m.

To reduce the number of "unknown level images" which would need to be compared against the training set, image metadata were used to filter the entire image set so that it only contained one image per day, acquired between 12:00 and 13:00, for the period between 22 November 2017 and 2 November 2018. This produced a set of 356 "unknown level images". The unknown set was loaded into the GIS and the water level in each image was compared against the water levels vector layer.

This process was imprecise. Camera shake introduced by wind, poor visibility, waves, and the large displacements caused by changes in the camera position introduced error estimated as at least ± 0.3 m. Two of the images in the training set, one acquired on the 21st January 2017 at 14:50 and one on the 30th of April 2017 at 17:22, appear to have exactly the same water level, but Hobo sensor depth readings within five minutes of each image acquisition are 1.775 m and 1.557 m respectively – figure 3.3.

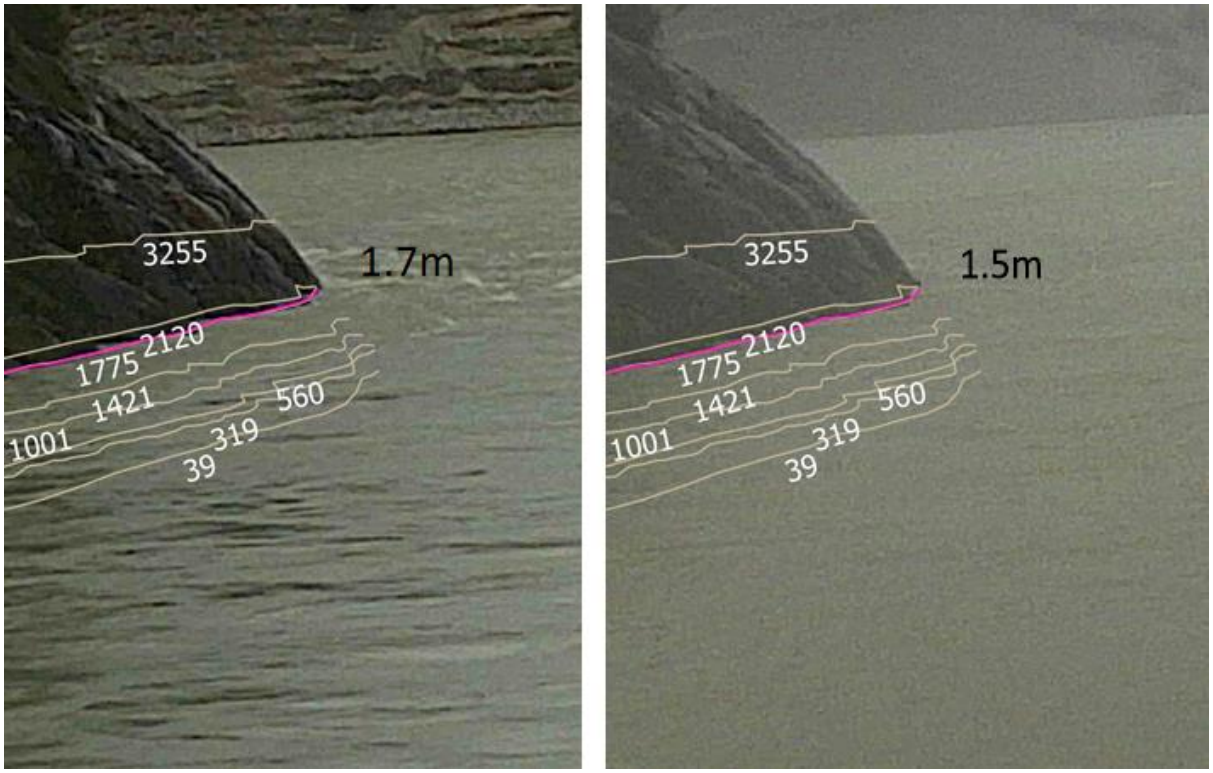

Figure 3.3: The water level in these images from the SpyPoint camera appears to be the same, however the corresponding HOBO reading for the right-hand image is a sensor depth of 1.775 m, while for the left-hand image it is 1.557 m.

3.2 Discharge modelling

3.2.1 The stage discharge relationship

The relationship between the water surface level or stage, of a river and its simultaneous discharge, which is the volume of water flowing through a cross-section in a given period of time, is a fundamental component of a catchment's water balance. The stage-discharge relationship is typically expressed as a rating curve, or simply a rating, which is derived from plotting stage in metres and discharge (Q), and typically fitting a power-law regression curve to the points, though in some cases 2nd or 3rd order polynomial curves are used and can provide acceptable results provided extrapolation above measured discharge is not needed (Birgand et al., 2013).

The equation of the curve intends to represent the stage-discharge relationship of the river for a given set of conditions, but uncertainty in field discharge measurement is large. Pressure sensors used to measure stage are affected by eddy currents during unsteady flow, and may be affected by sedimentation, vegetation, or dislodged by entrained debris. Significant error also exists in direct discharge measurements, especially in rivers where access and safety concerns mean the channel morphology cannot be measured precisely. Even when the most accurate measurements for stage and discharge are possible, the simple monotonic rating derived from these still does not account for water surface slope change during flood wave propagation and recession, known as hysteresis (Holmes, 2016; World Meteorological Organization (WMO), 2010).

Ideally, the rating is interpolated from discharge measurements covering the whole range of observed stages, but in rivers with extreme differences between low and high stage, especially where the flood regime is unpredictable, gauging discharge during high stage may be impossible so the rating must be extrapolated far above gauged measurements. This is a notoriously tricky problem and errors are often expected to be ± 50—100% at low flow and ± 10—20% for medium in-bank flow (McMillan et al., 2012), and up to ± 200% in some extrapolated sections (Kiang et al., 2018).

3.2.2 Existing gaugings in the Huemules River

Fluorometry or dye tracing is a commonly used method used for gauging river discharge. A known volume of a fluorescent tracer dye such as Fluorescein Sodium or Rhodamine B is injected into the water upstream of a sensor. As the water flows downstream, the concentration of the dye decreases due to dilution, dispersion, and decay. By measuring the concentration of the dye at the sensor, it is possible to calculate the discharge of the river (Kilpatrick and Cobb, 1985). Fluorometry is a relatively simple and inexpensive method of gauging river discharge, but it requires a well-mixed section of the river or tributary, and repeat measurements are key. Accuracy can also be affected by the presence of sediment, which can interfere with the measurement of the dye concentration.

In January, February and July 2017, a field team gauged discharge in the lower Huemules River using Rhodamine fluorometry (Marshall, 2020). Fourteen gaugings were made corresponding to Hobo sensor depth readings of between 0.72m and 2.02m, with calculated discharge values of between 59 and 209 m^3/s – table 3.1 and figure 3.4. These measurements cover most of the range of normal, i.e. non-GLOF water levels in the Lower Huemules River, but GLOFs such as those produced by Laguna de los Tempanos, can increase the water level by 8m or more. Figure 3.5 shows the dates of the dye tracing measurements against the Hobo sensor depth timeseries from August 2016 to August 2019. The two large peaks in sensor depth of over 8m and 6m in December 2016 and March 2017 respectively, show the huge difference between the range of discharge measured by dye tracing, and the likely discharge during GLOFs.

Table 3.1: Dates of dye trace measurements of flow velocity in the Lower Huemules River, and corresponding HOBO sensor depth readings.

Trace date	Hobo sensor depth (m)	Discharge (m^3/s)
2017-01-19	1.38	117
2017-01-22	1.68	145
2017-01-26	1.50	127
2017-01-27	2.02	209
2017-02-01	1.15	76.7
2017-02-03	1.41	99.5
2017-02-06	1.06	72.2
2017-02-09	1.07	76.8
2017-02-10	1.15	77.9
2017-02-11	1.40	116
2017-02-21	1.38	90.7
2017-07-20	0.72	59.4
2017-07-24	0.75	63.0
2017-07-27	0.87	72.4

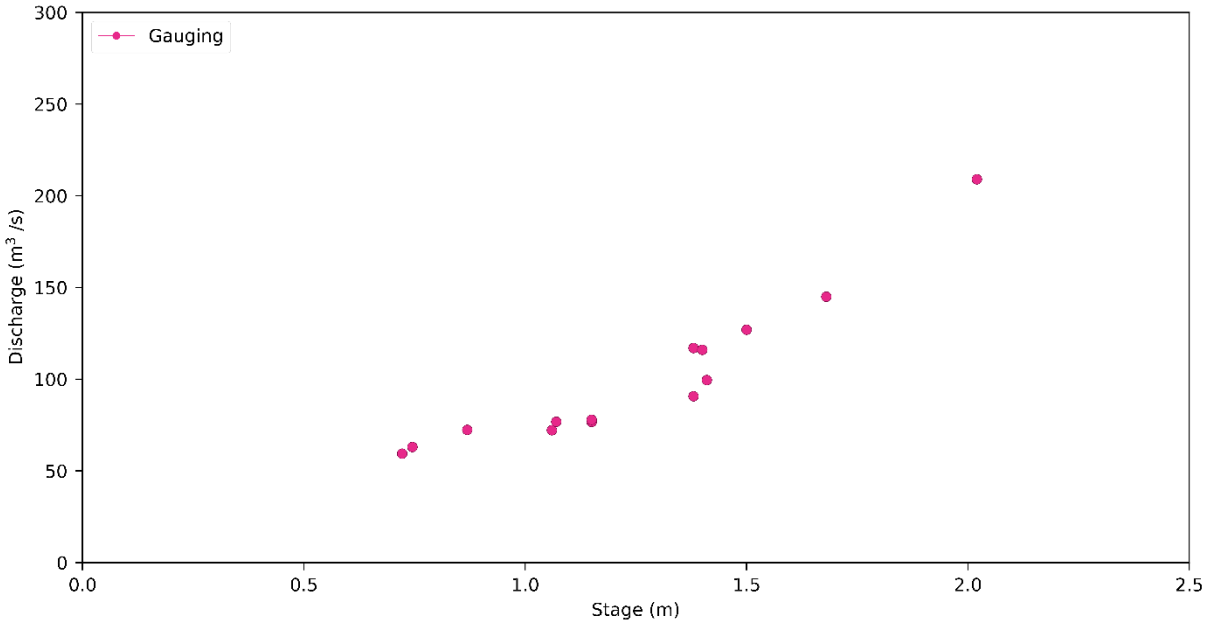

Figure 3.4: Gauged discharge from 14 Rhodamine B dye-injection traces completed during the 2017 field visits.

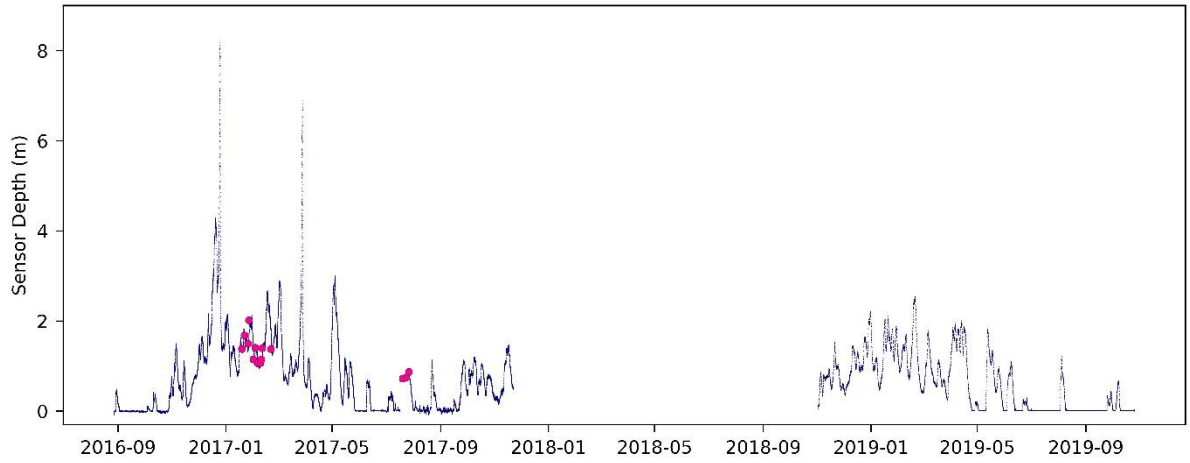

Figure 3.5: The dates of the 14 gaugings represented on the initial Hobo stage record, showing the huge increase in stage during GLOF events.

The stage discharge relationship over such a range is expected to be non-linear, due to reduced friction effects and increased channel width at high water, so constructing a rating on the basis of a regression to the gaugings alone may not accurately represent GLOF discharge. Figure 3.6 presents such an extrapolation by fitting a 2nd order polynomial regression to the gauged discharge values and extrapolating to GLOF stages. The peak sensor depth reading during the December 2016 GLOF was 8.2 m, which translates to a peak

discharge of 4503 m^3/s using this polynomial rating. Although the $r^2 = 0.97$ of the regression indicates a robust fit, the lack of physical basis for the rating at high stages puts this extrapolation in the realm of the "hydrological dragons" (Wagener et al., 2021).

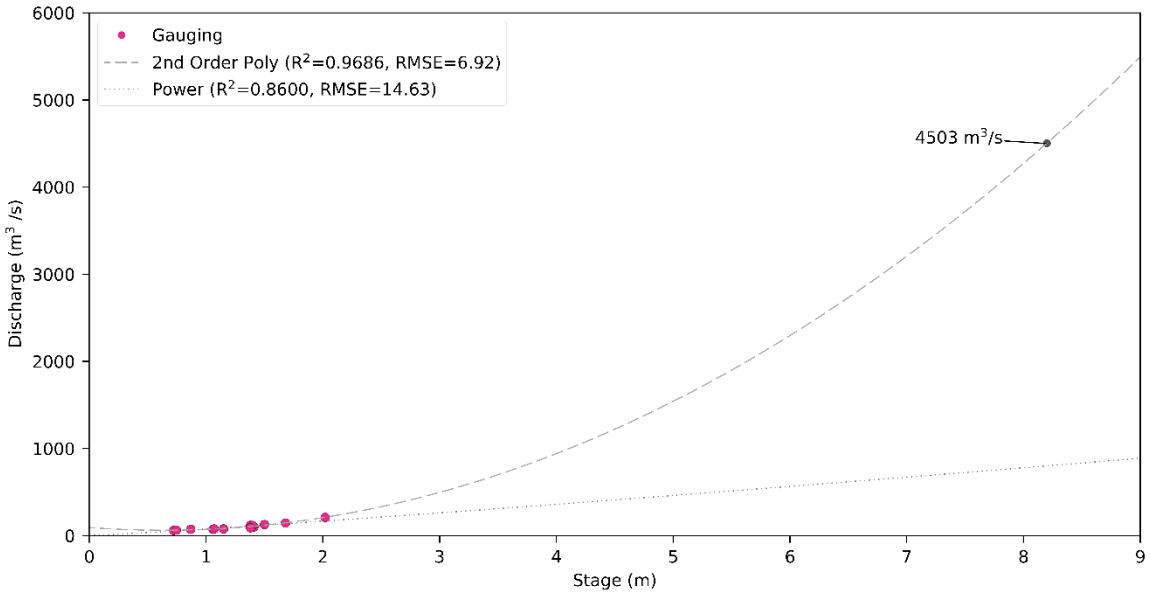

Figure 3.6: Ratings based on extrapolating a 2nd order polynomial regression and power-law regression from the 14 dye-trace gaugings. The label 4503 m3/s shows the discharge calculated at 8.2 m stage using the extrapolated polynomial.

Defining a physical basis for the rating above 2 m stage can help us improve the rating curve for the Huemules River until gaugings at high stage can be made. Time and equipment constraints during the field visit in October 2019 made it impossible to perform rigorous field surveys of the channel, so measurements of the river channel cross section, the slope of the modelled reach and the value of Manning's roughness coefficient were estimated using remote sensing and qualitative assessment of the channel characteristics based on photographs and recollections of the field visits. Considering the error expected in these measurements and estimates, a simple discharge model based on the velocity area method was considered suitable rather than more mathematically complex options (Herschy, 1993).

3.2.3 Channel cross-section

Fortunately, remotely sensed data is available showing the channel during the early stages of the March 2017 GLOF, and this allowed an assessment of the flow at medium to high stage. Based on Sentinel-2 images, and other high resolution imagery, the channel was measured near a suggested hydraulic jump at the end of the bedrock reach at times corresponding to low (0.182m) and high (3.50m) sensor depth readings – figure 3.7. Above a sensor depth of 3.50m, the full channel is approximately 65m wide, but at lower flows bedrock outcrops split the channel, leaving a roughly 40m wide main channel and a 10m wide side channel that is probably shallower. The outcrop is about 15m across. These estimates were used to build a compound model for the cross-sectional area which increases non-linearly with stage – figure 3.8.

The sensor depth time series in figure 3.5 shows that the Hobo sensor repeatedly recorded zero or close to zero depth during low flows in the winter and autumn months. When the last field team downloaded data from the HOBO in October 2019, the final 24 hours of depth readings averaged just 0.015m, but throughout this time there was substantial flow in the river, as shown in photographs of the channel taken while re-installing the sensor – figure 3.2. Without measurements of the channel depth, a visual estimate was made that the average channel depth at the bedrock constriction was around 70 cm deeper than the elevation of the Hobo.

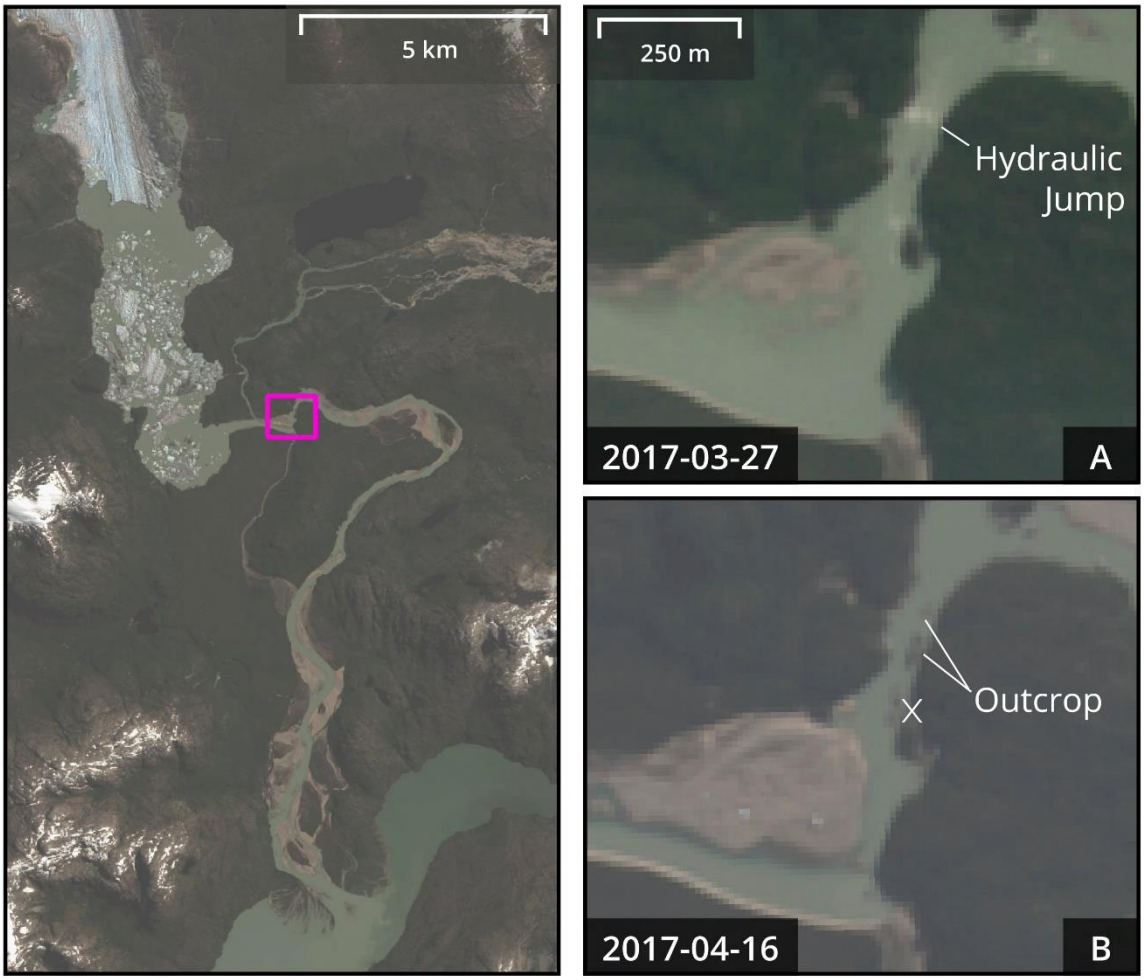

Figure 3.7: Sentinel-2 imagery of the Lower Huemules river under different flow conditions. Image A corresponds to a HOBO sensor depth of 3.50 m during the early stages of the March 2017 GLOF. A patch of white water at the end of the bedrock reach is proposed to represent a hydraulic jump, indicating transition to critical flow. Image B corresponds to a sensor depth of 0.18 and bedrock outcrops that split the channel are labelled. The position of the Hobo sensor is marked with an X.

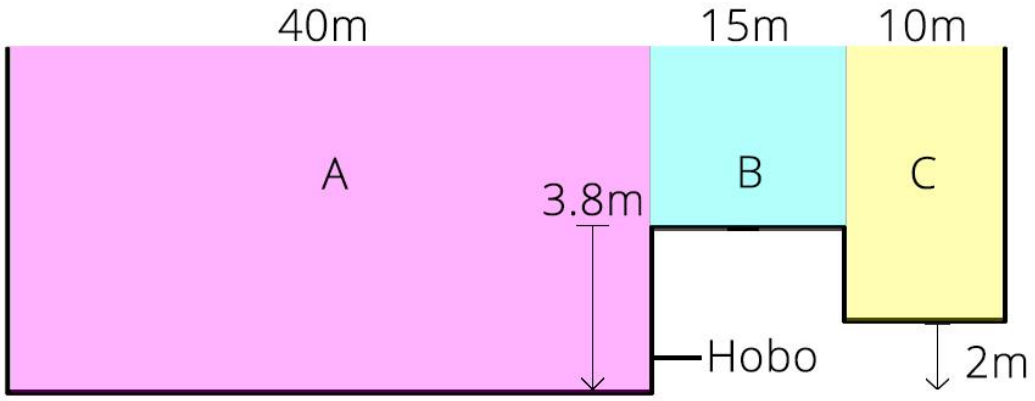

Figure 3.8: A simplified channel cross-section, showing the main channel (panel A), the side channel created by the outcrop (panel C) and the additional area which carries flow once the outcrop is overtopped at around 3.8 m water depth (panel B). The approximate relative elevation of the Hobo is labelled. The location of this cross-section corresponds to the end of the bedrock channel at the hydraulic jump labelled in figure 3.8.

3.2.4 Valley slope

The valley slope along the bedrock reach was estimated using the 30 m resolution Shuttle Radar Topography Mission (SRTM) digital elevation model (DEM). This is a very crude approximation of slope, and does not represent water surface slope which is the requirement for Manning's equation, but as a starting point for model calibration these limitations were accepted. Figure 3.9 shows the SRTM DEM of the bedrock reach and elevations sampled from within the two red polygons. Calculating slope based on the difference between the minimum and maximum elevations recorded in each polygon produced a maximum slope of 0.005 and a minimum of 0.002.

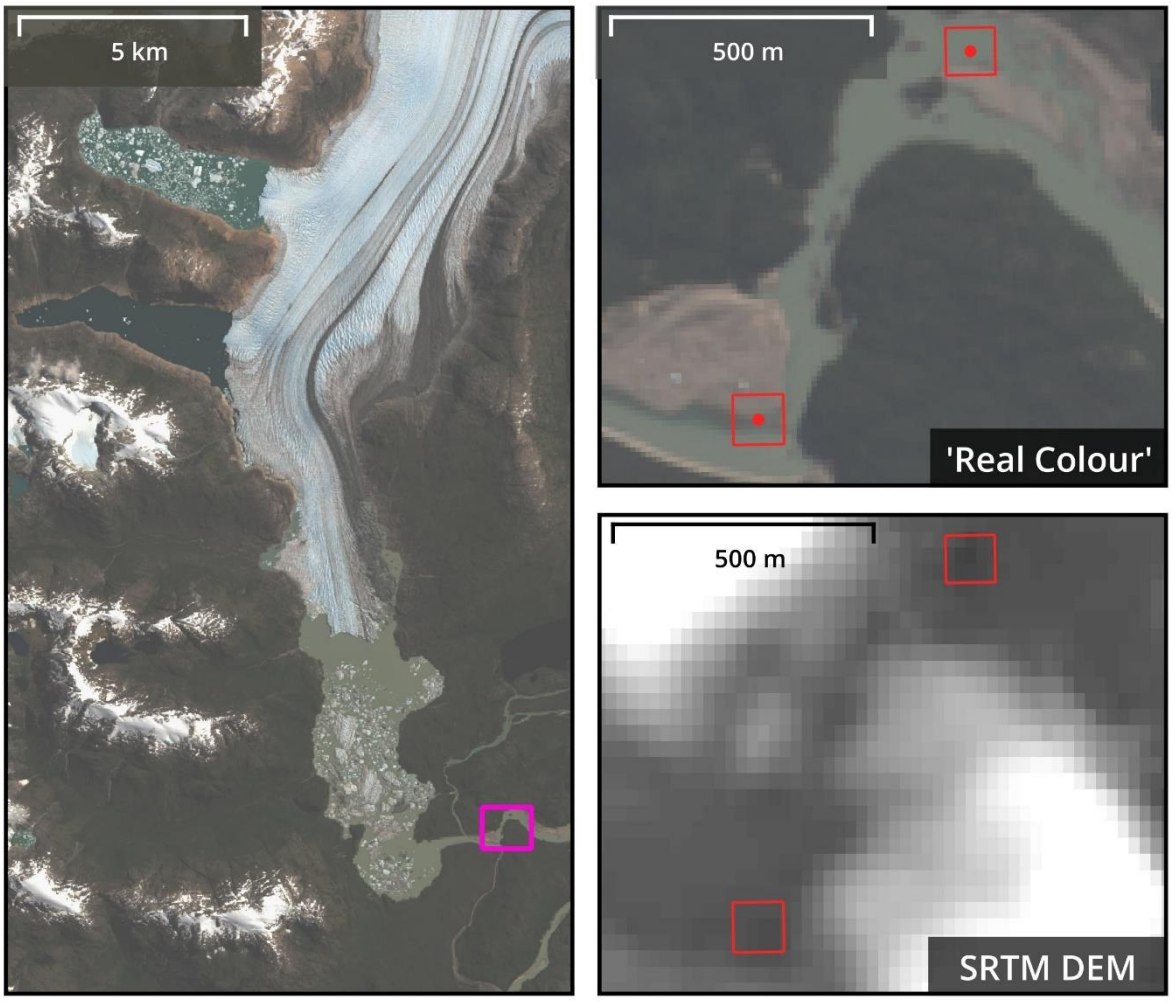

Figure 3.9: Estimating valley slope using the SRTM DEM. This is a hideously crude estimate, but it resulted in a believable value which was accepted as a starting point for model calibration.

3.2.5 Bed roughness and flow conditions

Manning's roughness coefficient was estimated to be 0.035 after following the step-by-step procedure described in Arcement and Schneider (1989) and comparison with channels described in Barnes (1967). Although we had no direct evidence of the bed material, based on the composition of the riverbanks and in-channel bars we expect this reach to contain sand and gravel, possibly cobbles, which may be scoured to bedrock during extreme discharge events.

3.2.6 Accounting for uncertainty in the physical variables

To account for uncertainty in the estimates for slope and Manning's n, a lower flow velocity bound was modelled with a slope of 0.0035 and n of 0.05, and an upper bound was modelled using a slope of 0.005 and n of 0.035. These were iteratively tested for their ability to produce an envelope model that best captured all the gauged discharge values, as described in the following sections. The variables chosen for the model are presented in table 3.2.

Table 3.2: Final physical variables chosen for input into the Manning's based velocity area discharge model.

	Slope	Manning's n
Q_{low}	0.0035	0.05
Q_{best}	0.0042	0.04
Q_{high}	0.0050	0.035

3.2.7 Estimating a physical maximum discharge

As shown in figure 3.7, at sensor depth readings around 3.5 meters and over, white water fills the channel constriction as it flows from the bedrock channel into the wider pool at the meander. This could indicate a transition to supercritical flow in the narrowest section of the river below the HOBO sensor followed by a hydraulic jump. Under this assumption the HOBO water level would be controlled by the water transitioning from sub-critical to critical flow, and therefore a Froude number of ≥ 1, the physical maximum discharge at various water levels could be calculated by using the channel cross-section from figure 3.8 and the Froude equation to find flow velocity: $v = \sqrt{gD}$, where g is acceleration due to gravity (9.81) and D is the flow depth.

The satellite imagery is a very limited source for this interpretation and if no transition to supercritical flow occurs then the actual flow in this part of the channel will be less than this

critical flow prediction. Considering this uncertainty, the critical flow prediction serves as a physical maximum bound for discharge in the bedrock channel, and a sense check in case the model outputs unreasonably high discharge estimates.

3.2.8 Model calibration

To estimate discharge (Q) for creating an envelope rating curve, flow velocity (V) was modelled using Manning's equation. Because the Huemules channel is much wider than it is deep, depth (d) was substituted for the hydraulic radius to simplify the calculation:

$$V = \left(\frac{1}{n}\right) d^{2/3}\sqrt{S}$$

The values for slope (S) and Manning's roughness coefficient (n) were taken from table 3.2 to generate upper and lower bounds alongside a best estimate of discharge. Velocity was modelled for depths from 0.1 m to 2.1 m for each panel of the compound channel model. These panels are the 40m wide main channel (a), which always carries flow; the 10m wide side channel (c), which is assumed to carry flow when main channel depth reaches 2m or over; and the 15m width of the boulder (b), which is overtopped at around 3.8m depth – figure 3.8. Discharge (Q_a, Q_b, Q_c) was then calculated using the velocity-area method where width for each panel is W_a, W_b and W_c. Discharge in the three panels was summed to provide an overall discharge estimate that considers the changing channel cross section as depth increases:

$$Q_a = VdW_a$$

$$Q_b = if\ (d \geq 3.8)\ \{V(d - 3.8)W_b\}\ else\ (d < 3.8)\ \{0\}$$

$$Q_c = if\ (d \geq 2)\ \{V(d - 2)W_c\}\ else\ (d < 2)\ \{0\}$$

$$\boldsymbol{Q} = Q_a + Q_b + Q_c$$

The lower bound (Q_{low}), best estimate (Q_{best}) and upper bound (Q_{high}) discharge models were iterated by adjusting the slope and roughness coefficient inputs until the best estimate fit the

dye trace points up to the highest dye-traced gauging at just over 2 m sensor depth. To account for scatter in the gauged discharge, the Q_{low} and Q_{high} models were calibrated to create an envelope which captured all the gauged points, apart from the three gaugings made at less than 1 m stage, since channel effects are expected to become more pronounced at very low stages – figure 3.10. This model calibration was done qualitatively because a more formal approach (least squares or similar) is unlikely to give a better outcome given the limited calibration data.

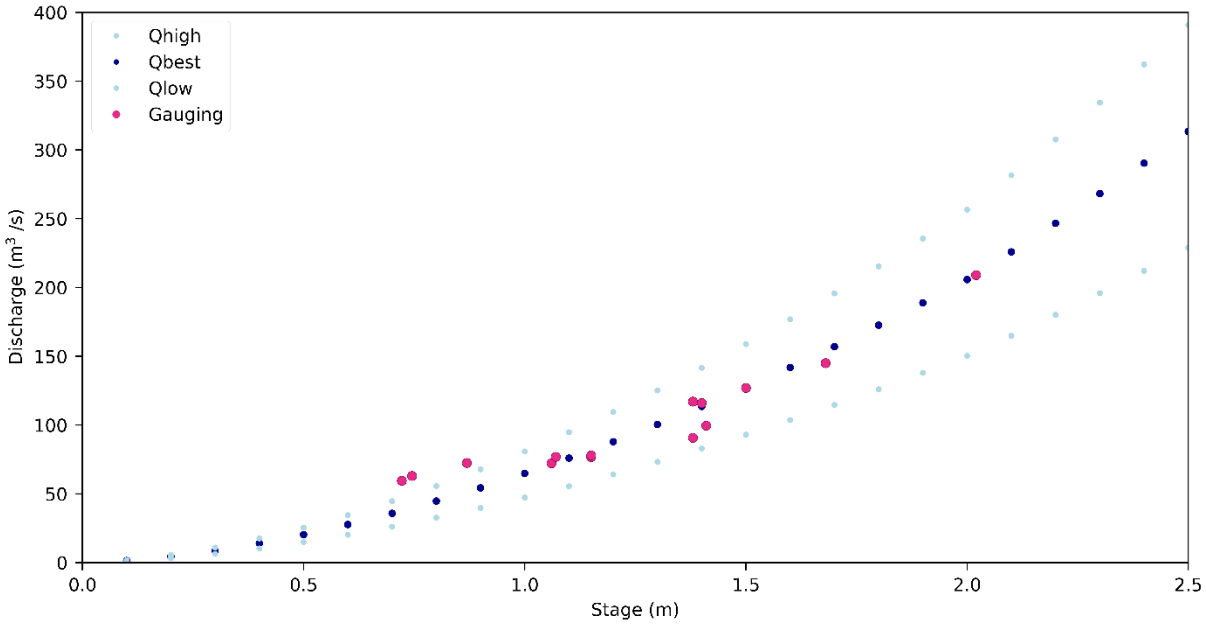

Figure 3.10: Between 1.0 and 1.5 m stage the envelope model captures all the 2017 gaugings, and up to 2.0 m stage the model best estimate (Qbest), fits the gauged points well.

Extending the envelope model to high GLOF stages of more than 8 m shows that the best estimate discharge model indicates GLOF discharge of around 3000 to 3800 m^3/s between stages of 8 and 9 m, while at stage = 8.5 m, the critical flow prediction indicates a physical maximum discharge in the channel of 4800 m^3/s and the polynomial rating exceeds this, giving a discharge of 4862 m^3/s – figure 3.11.

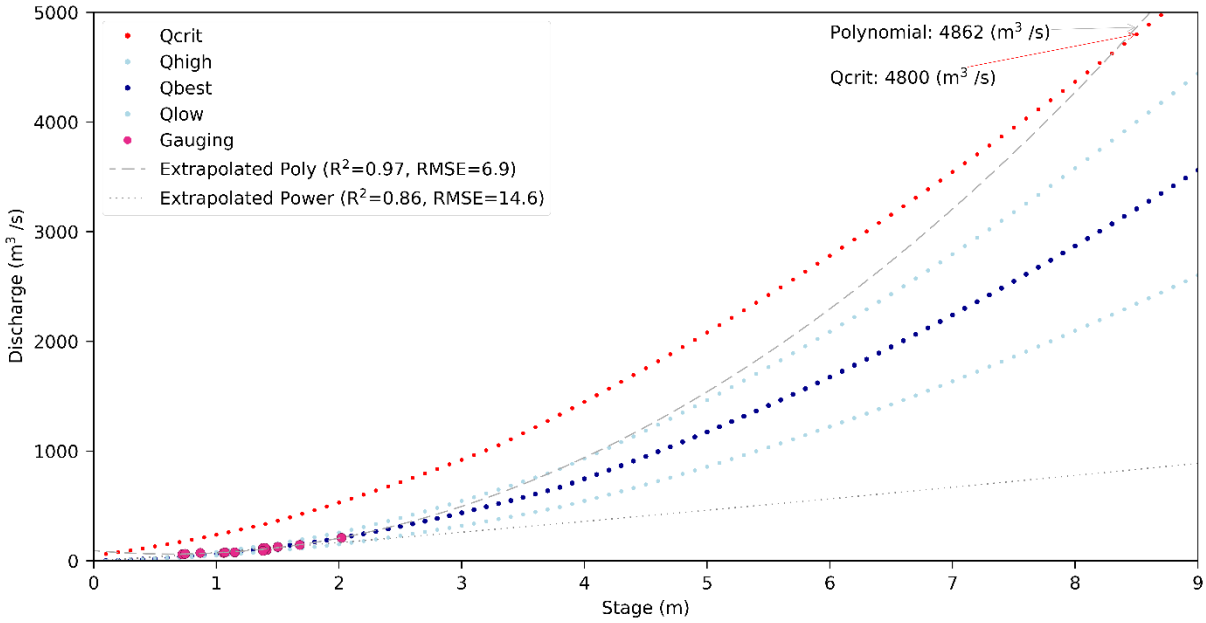

Figure 3.11: The extended discharge models plotted alongside discharge under the critical flow assumption (Qcrit), and the extrapolated power and 2nd order polynomial ratings.

3.3 The equation of the rating curve

As described in section 3.2.8, modelling discharge using a compound channel produces values close to gauged discharge in the Lower Huemules River at non-flood stages, and at high stage the model stays well below our critical flow assumption for the physical maximum discharge. By extending the discharge models to GLOF stages of >8 m and fitting a power-law regression curve to the resulting points, a series of ratings is produced to give a lower bound (Q_{low}), best estimate (Q_{best}) and upper bound (Q_{high}) for the stage-discharge relationship.

$$\boldsymbol{Q_{low} = 47.8d^{1.8}}$$

$$\boldsymbol{Q_{best} = 65.5d^{1.8}}$$

$$\boldsymbol{Q_{high} = 81.7d^{1.8}}$$

Where **Q** is discharge in m^3/s and **d** is Hobo depth + 0.7 m.

3.4 Rating corroboration

As described in section 2.2, the Clague—Matthews relationship provides an estimate of the peak discharge through a subglacial conduit given the total volume of the source lake: $Q = 75\ V_t^{0.67}$ where Q is discharge in m^3/s and V_t is the source lake volume in $m^3 \times 10^6$ (Clague and Mathews, 1973; Ng and Björnsson, 2003; Walder and Costa, 1996). By finding the pre-GLOF volume of the Laguna de los Tempanos, and using the Clague—Matthews relationship, it should be possible to generate estimate for peak GLOF discharge during the December 2016 and March 2017 events, and so use these estimates to corroborate the modelled rating at high stage.

Because no bathymetry exists for the glacial lakes, an indirect measurement method was necessary for estimating source lake volume. Empirical scaling relationships between lake surface area and volume have been tested in a variety of alpine settings (Cook and Quincey, 2015; Huggel et al., 2002) and recently used to show that glacial lake volume in the Northern Patagonian Icefield increased by 66.0 km^2 between 1945 and 2011 (Loriaux and Casassa, 2013).

The water surface area of the Laguna de los Tempanos is heavily shadowed by the high topography north of the lakes, which makes it difficult in many cases to delineate the water surface in optical imagery acquired during the austral autumn, winter and spring. Use of the normalised difference water index (NDWI) as discussed in (DeAlwis et al., 2007; Bolch et al., 2008; Frey et al., 2010; Gardelle et al., 2011) mitigates much of this issue where cloud free images are available – figure 3.12.

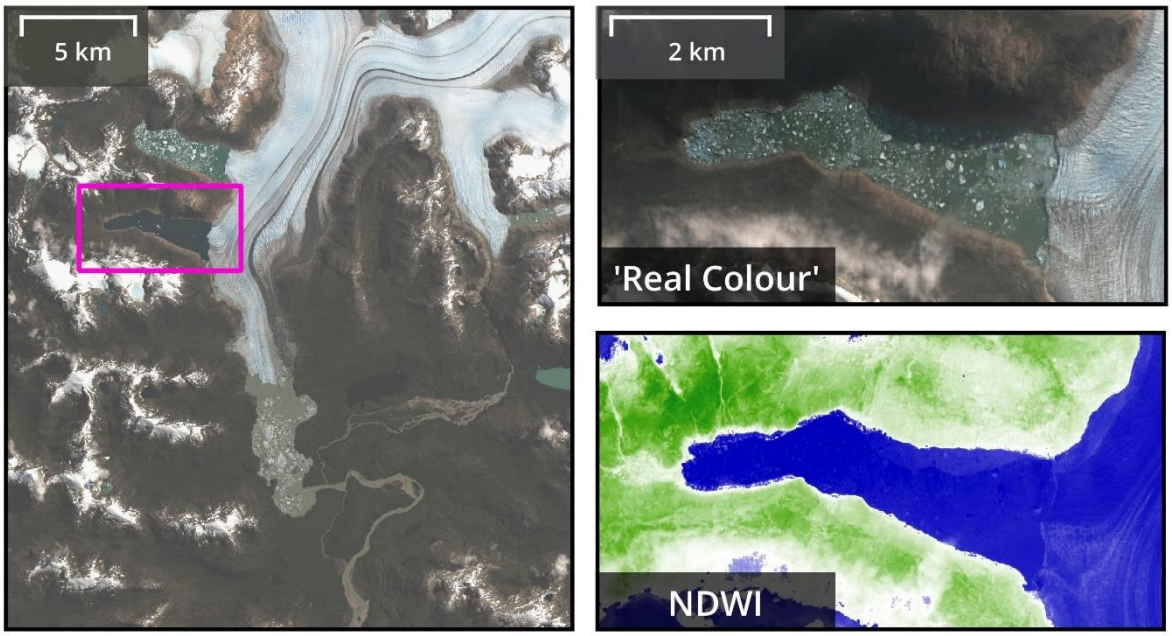

Figure 3.12: Illustration of shadow in optical satellite imagery of the Laguna de los Tempanos. The Sentinel 2 acquisition was made on the 27th of March 2017, during the early stages of the GLOF. The 'real colour' image shows how shadowing can complicate lake delineation.

Shadow affects SAR imagery as well, although in this case it is caused by steep topography blocking the generated radar signal from reaching areas of the surface. Because water has a high dielectric constant and an often smooth surface, the incoming microwaves are reflected away from the sensor effectively, resulting in very low backscatter. This means that still, ice-free surface water is almost indistinguishable from radar shadow, and water surface delineation is more difficult. No cloud free optical imagery of the Laguna de los Tempanos is available prior to the December 2016 GLOF, but a Sentinel 1 SAR image acquired on the 20th of December 2016 allows a measurement of lake surface area – figure 3.13. In this image, floating brash ice and bergs make it easier to define the lake shore from areas of radar shadow.

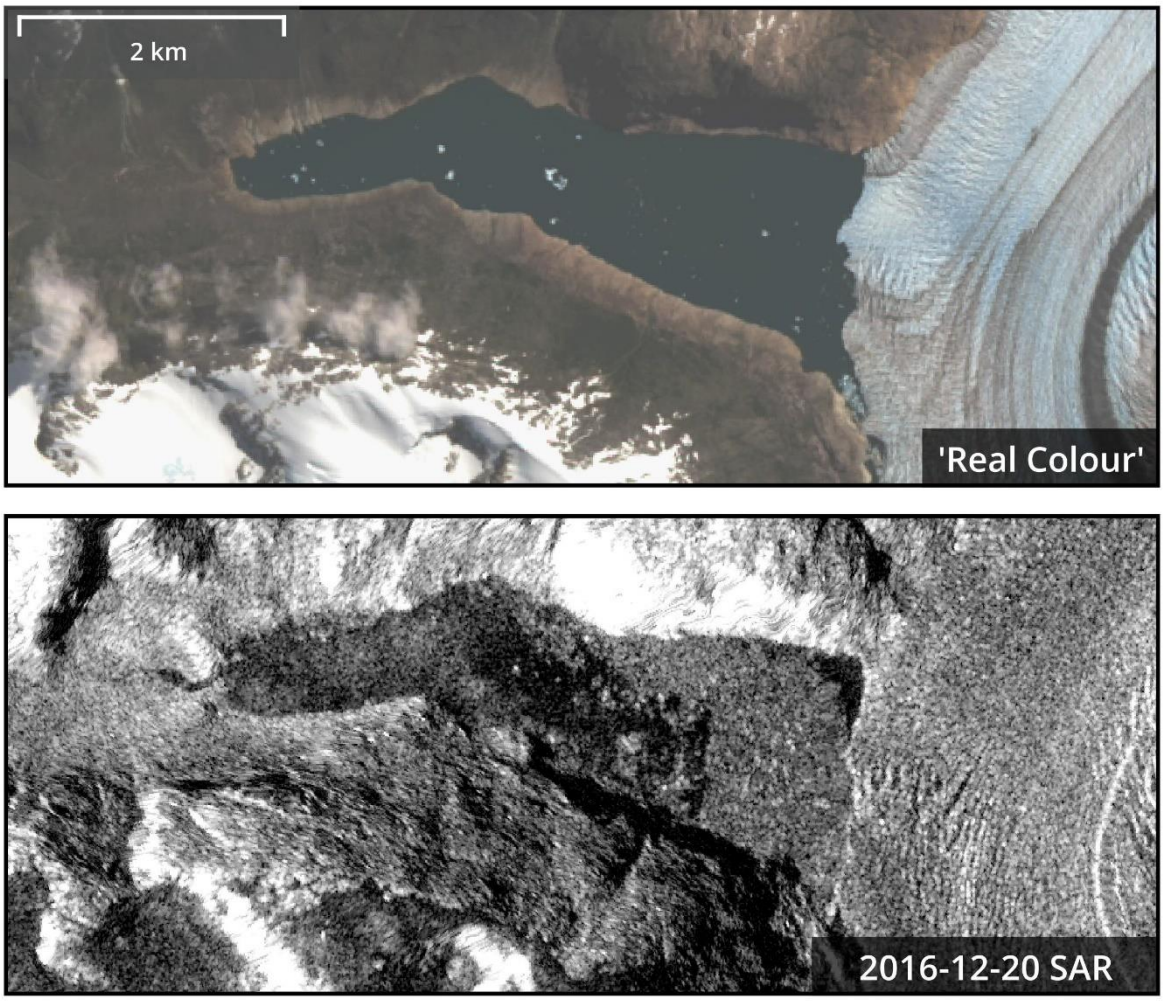

Figure 3.13: Comparison of Landsat optical satellite imagery and Sentinel 1 SAR imagery to show how radar shadow can complicate lake surface measurements.

By measuring lake surface area using the NDWI and SAR images presented in figures 3.12 and 3.13, the Laguna de los Tempanos was measured at 5,097,204 m^2 for a volume of 253.6×10^6 m^3 prior to the December 2016 GLOF, and 4,438,670 m^2 for a volume of 210.9×10^6 m^3 prior to the March 2017 GLOF using surface area to volume relationships tested for the Northern Patagonian Icefield (Loriaux and Casassa, 2013).

Using these source lake volumes, the Clague—Matthews relationship predicts peak conduit discharge to be 3061 m^3/s for the December 2016 GLOF and 2705 m^3/s for the March 2017 GLOF. The average gauged discharge for the Lower Huemules during January and February 2017 was 110 m^3/s, so peak discharge in the Lower Huemules may be estimated at

3171 m³/s and 2815 m³/s for the December and March GLOFs respectively. Plotting these estimates on the modelled envelope rating shows these discharge estimates fall within the expected range for discharge given by the model, and therefore provide some physical corroboration for the model at high stage – figure 3.14.

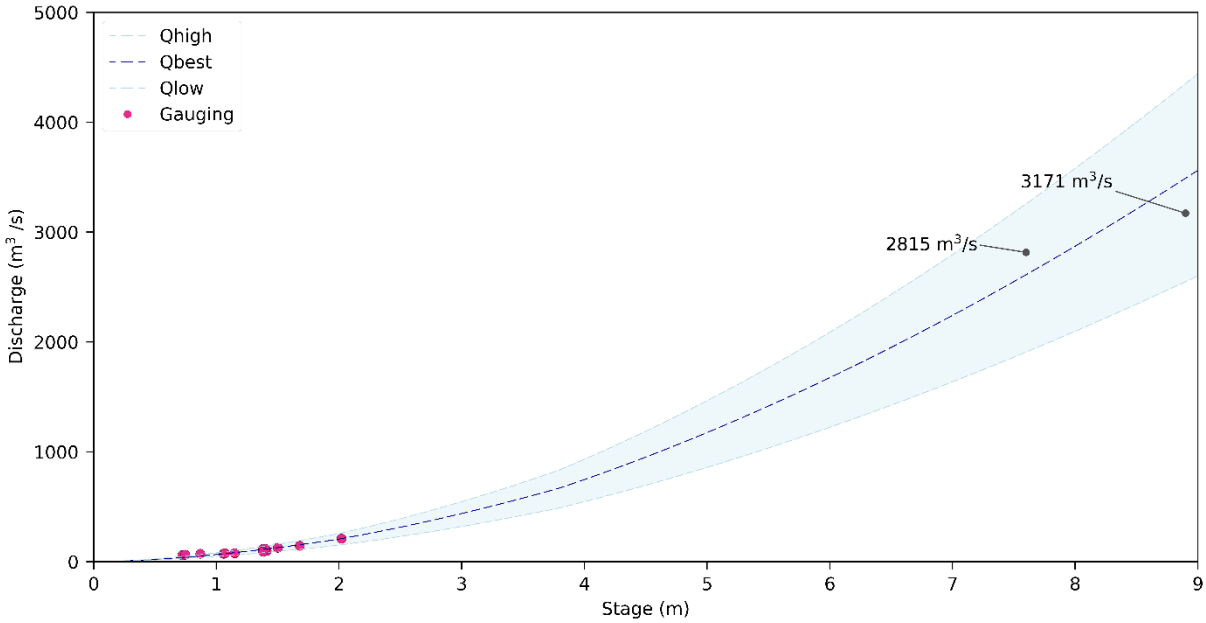

Figure 3.14: The envelope rating for the Lower Huemules River with calculated Qmax for the December 2016 and March 2017 GLOFs plotted.

3.5 Summary of methods

Water pressure data and time-lapse photographs of the Lower Huemules River were used to create a continuous six-year record of channel depth. Remotely sensed data from SRTM and Sentinel-1 and 2 were used to estimate the channel cross-section and slope, and the water surface area of the Laguna de los Tempanos. Discharge in the Lower Huemules was modelled using Manning's equation and the velocity-area method, and the model tested at low stage by comparison with observed discharge from dye-tracing measurements performed by a previous field team, and at high stage by comparing GLOF Qmax predicted by the Clague—Matthews relationship to the envelope rating.

4 Results

This section uses the best estimate rating with error bounds of ± 25% to describe discharge in the Lower Huemules River between September 2016 and April 2022. General trends in the discharge record are described first, introducing mean monthly and annual discharge, then individual high flow events are discussed in relation to precipitation records and known GLOFs from the satellite record. Three GLOFs from the Laguna de los Tempanos and GL3 are described, and the volume of water released during those events is calculated from the discharge record and verified by comparison against satellite derived estimates of lake volume where possible. Each GLOF hydrograph is discussed with reference to potential drainage pathways and their influence of the hydrograph shape. Using recent knowledge on the thinning rate of Steffen Glacier, future GLOF hazard from the Laguna de los Tempanos, GL1 and GL3 is discussed with reference to projections for glacier mass loss in the NPI under climate change scenarios.

4.1 GLOF characteristics and discharge in the Lower Huemules River

4.1.1 General trends

Between September 2016 and April 2022 discharge in the Lower Huemules River exhibits a distinct seasonality with peak flows occurring in the austral summer between November and June. At least five GLOFs are indicated by the discharge record, in December 2016, March 2017, May 2021 and January 2022. The GLOF in December 2016 was the largest of these with discharge measured at 3432 m^3/s ± 25%. Since that event, GLOF magnitude has declined – figure 4.1. Mean annual peak discharge, excluding verified GLOF events, is 650 m^3/s ± 25%, so the largest GLOF events result in discharges around five times the mean annual peak.

Between late 2017 and late 2018, the Hobo pressure transducer failed to record and visual estimates of stage were made using daily photographs of the river. These data have low

temporal resolution (24 hours) and large potential error (approximately 40 percent at 1.3 m stage and 12 percent at 4.3 m stage), but still represent a realistic record of discharge.

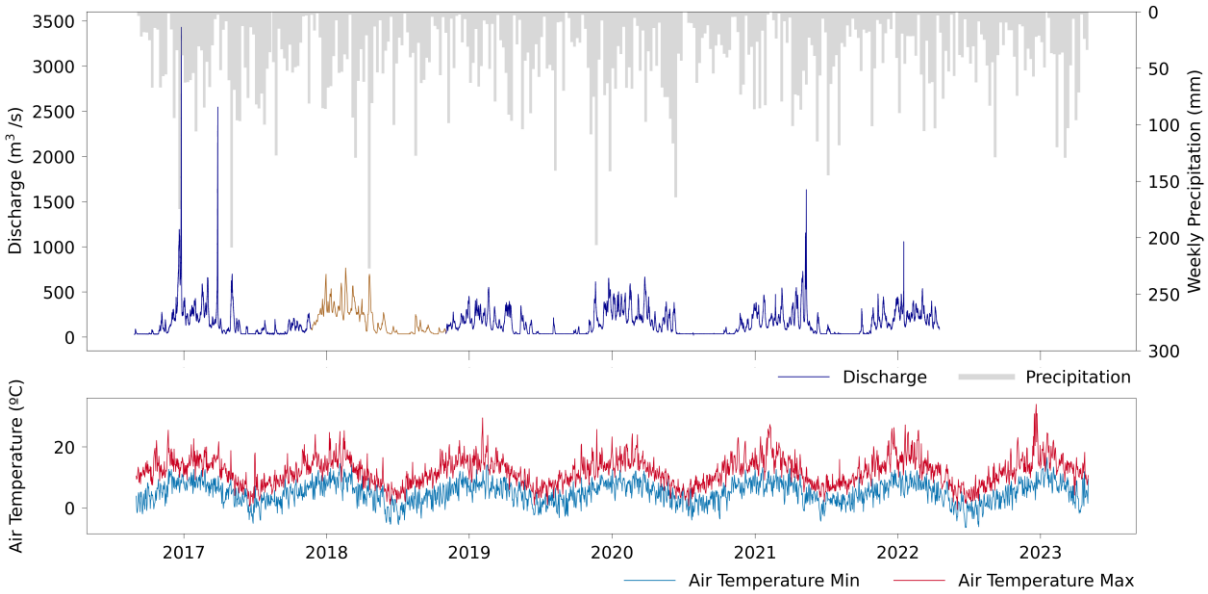

Figure 4.1: Discharge in the Lower Huemules River plotted with weekly accumulated precipitation and daily air temperature min/max measured at the weather station in Caleta Tortel approximately 30 km south-southeast. The dark orange representation of discharge between late 2017 and late 2018 represents where the Hobo sensor failed to record, and stage was estimated visually from daily photographs of the channel. Mean annual peak discharge, excluding verified GLOF events, is 650 m^3/s ± 25%.

The discharge record during austral winters, roughly June – October, is incomplete due to water level in the river regularly dropping below the installed Hobo pressure transducer, so mean and minimum discharge for those months is unavailable, although peak flows are recorded and show that isolated high precipitation events can cause flow to temporarily reach more than 300 m^3/s, which is higher than the typical summertime mean discharge. Figure 4.2 shows that the highest monthly mean and median discharge is recorded in December, January and February. Despite no large GLOFs recorded during January and February, mean and median discharge recorded during those months is still higher than in March and May, when GLOFs have been recorded.

From its winter low in August and September, discharge increases rapidly at the beginning of the warm season as snowmelt feeds into the river from the catchment area. Mean

discharge stays above 150 m^3/s until June, when it drops sharply as precipitation begins to accumulate as snow at most elevations. Mean summertime discharge from 2016 to 2022 has varied by up to 100 m^3/s between different years. Table 4.1 below shows mean and median values for discharge during the November – June period of each austral summer from 2016-2017 to 2021-2022.

Table 4.1: Mean and median summer discharge in the Lower Huemules River between 2016 and 2022.

Year	Summer Mean (m3/s)	Summer Median (m3/s)
2016-17	253	188
2017-18	149	105
2018-19	179	159
2019-20	249	220
2020-21	208	166
2021-22	230	216

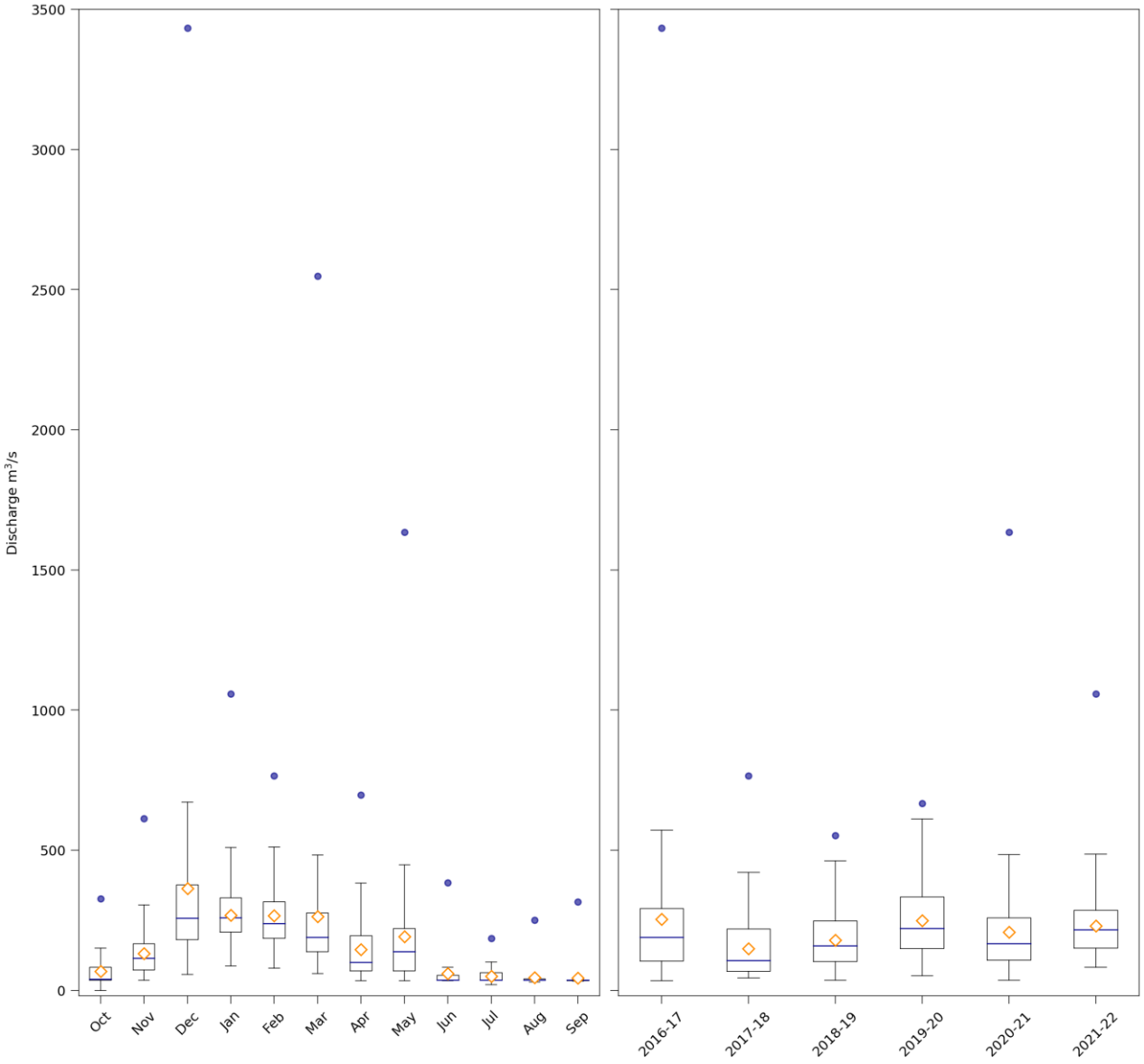

Figure 4.2: Boxplots showing monthly, and summer seasonal discharge in the Lower Huemules River between October 2016 and April 2022. The median discharge is represented by a blue horizontal line in the box, and the mean is shown as a hollow orange diamond. The peak discharge recorded is shown by the blue circle.

The huge difference between peak and mean flows during GLOF and non-GLOF years is well illustrated by figure 4.2. As previously mentioned, the largest GLOF measured in the discharge record in the Huemules river was 3432 m^3/s ± 25% between the 24th and 26th December 2016. The next highest discharge occurred during the same summer, at the end of March. No major GLOFs were recorded in the following three summers, and the peak annual discharge is much closer to the middle 50 percent.

4.1.2 2016 to 2017

The summer of 2016 to 2017 is the start of discharge measurement in the Lower Huemules River and contains the two largest GLOF events in the record – figure 4.3.

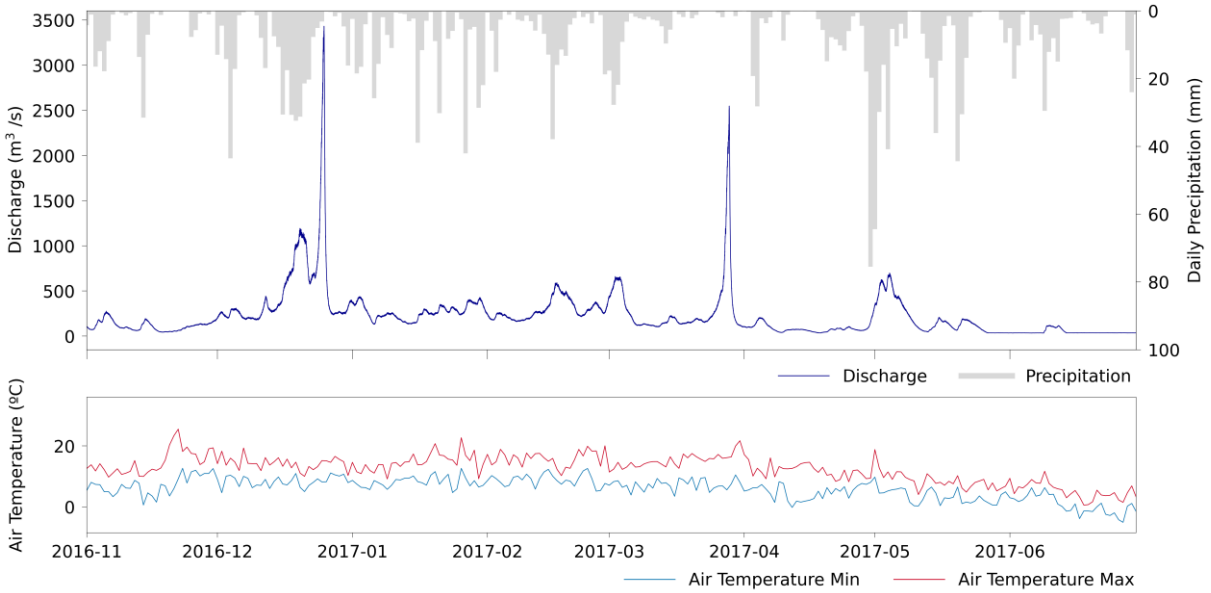

Figure 4.3: Discharge in the Lower Huemules River plotted with daily accumulated precipitation and daily air temperature min/max measured at the weather station in Caleta Tortel approximately 30 km south-southeast.

Figure 4.3 clearly illustrates the relative magnitude of the two GLOFs recorded at the end of December 2016 and end of March 2017. Air temperature measured in Caleta Tortel does not indicate warm periods act as a trigger for lake outburst, and precipitation, while clearly linked to discharge, is similarly inconclusive as a GLOF predictor. The December GLOF is preceded by a prolonged period of rainfall and a marked discharge peak of over 1000 m^3/s, before the rapid spike in discharge occurs as the Laguna de los Tempanos emptied fully, but the March 2017 GLOF is preceded by a dry period. Closer examination of the hydrograph leading up to and including the December GLOF shows the initial increase in precipitation happened over about four days and is somewhat stepped, closely following the substantial daily precipitation – figure 4.4.

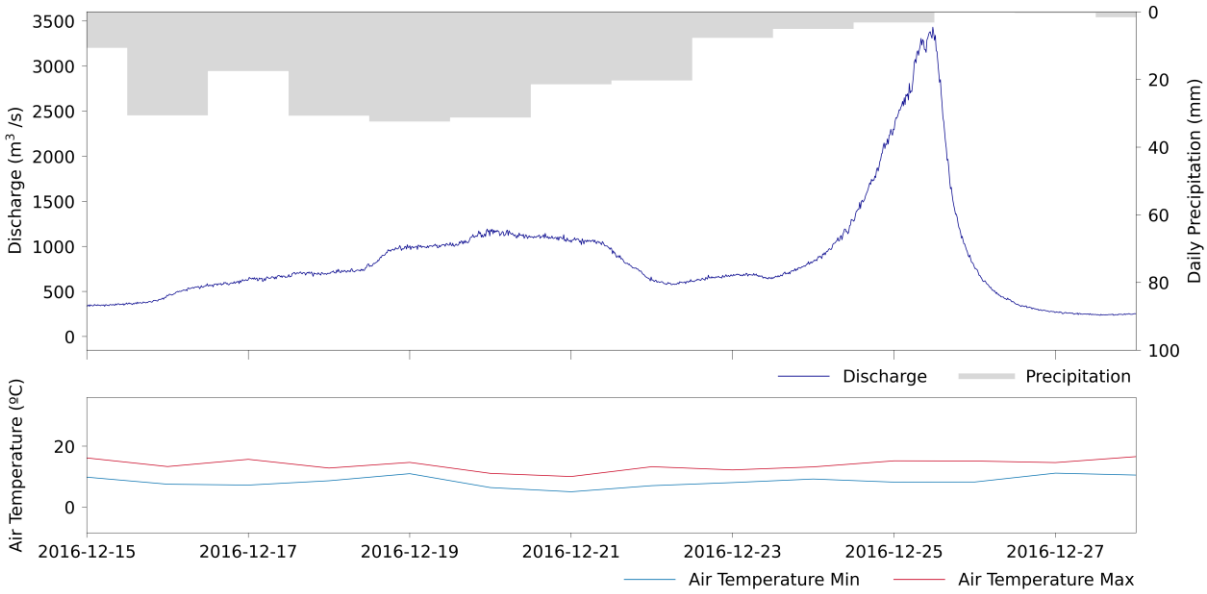

Figure 4.4: Discharge and precipitation preceding and during the December 2016 GLOF.

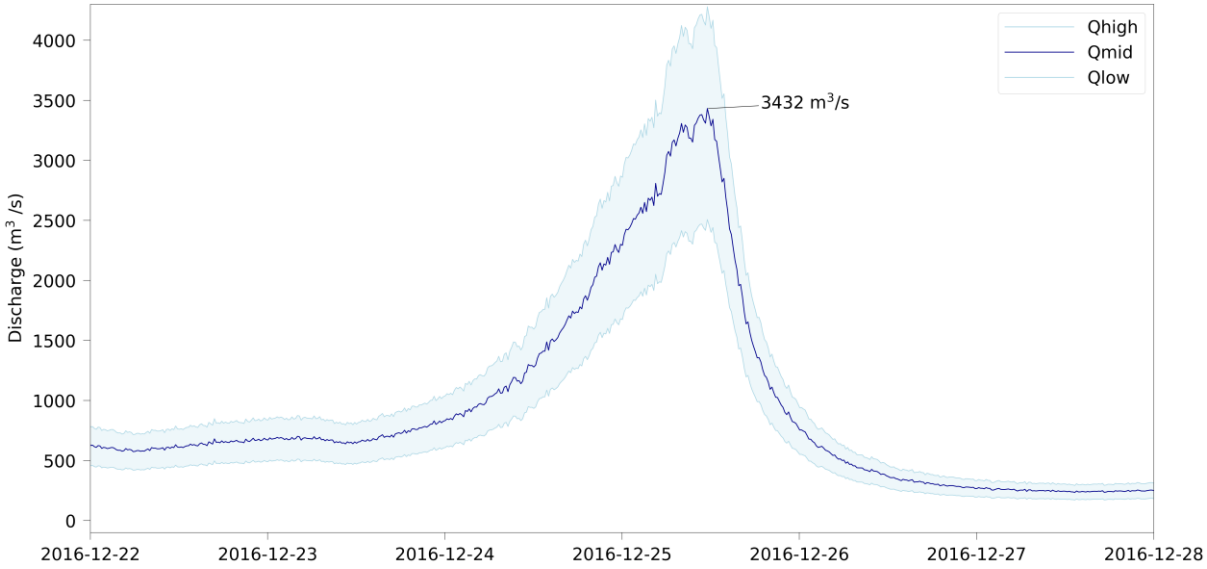

Figure 4.5: GLOF hydrograph for the December 2016 outburst from the Laguna de los Tempanos. The light blue shaded area shows the range between the lower and upper bounds estimated by discharge modelling, and the dark blue line represents the best estimate of discharge. Peak discharge was 3432 m^3/s ±25% recorded on 2016-12-25 11:33.

The GLOF hydrograph in figure 5 follows the classical form for outburst flood discharge enlarging a sub-glacial conduit by frictional melting. The rising limb of the hydrograph begins gradually and increases roughly exponentially to its peak over about 48 hours, before collapsing. Peak discharge was approximately 3432 m^3/s, with the lower and upper bounds

giving a range between roughly 2500 to 4200 m^3/s. These values for GLOF discharge are similar to the median values estimated from lake gauging for the Cachet 2 GLOFs reported by Jacquet et al. (2017) to be around 4300 m^3/s.

Remotely sensed imagery from the Sentinel 1 satellite shows a partial drainage of the Laguna de los Tempanos between the 2nd and 20th of December – figure 4.6. In synthetic aperture radar (SAR) imagery, smooth open water appears black because the emitted microwave radiation is reflected away from the sensor, while ice, earth and vegetation appear as shades of grey because they scatter the incoming microwaves and reflect a portion back to the sensor. Spaceborne SAR instruments are "side looking" and emit microwaves at an oblique angle to the Earth surface rather than straight down towards the nadir. When steep terrain results in a slope facing towards the incoming signal it results in very strong reflection back to the sensor which appears as bright white in the resulting image. This is visible in the three SAR images in figure 4.6, because the images were acquired on an ascending orbit and the microwave beam was directed to the right of the instrument, so incident on the ground from left to right across the image. In figure 4.6 the drainage of the Laguna de los Tempanos in December 2016 is evident in the SAR timeseries presented on the right of the figure. Brash ice and icebergs give the lake surface a patchy grey appearance, but clear water is visible in a small basin at the western end of the lake in the image from the 2nd of December. On the 20th of December that small basin has drained, indicating that partial drainage of the lake contributed to the high discharge event prior to the main outburst commencing late on the 23rd of December. The final image in the timeseries, acquired on the 26th of December at 19:56 local time, the valley bottom appears dry with no open water visible. The resultant ice cliff is indicated by a line of strong backscatter (bright white) identified by the pink arrow. This indicates the Laguna de los Tempanos was entirely drained by the December 2016 outburst, with the face of the ice cliff generating a strong return signal to the sensor.

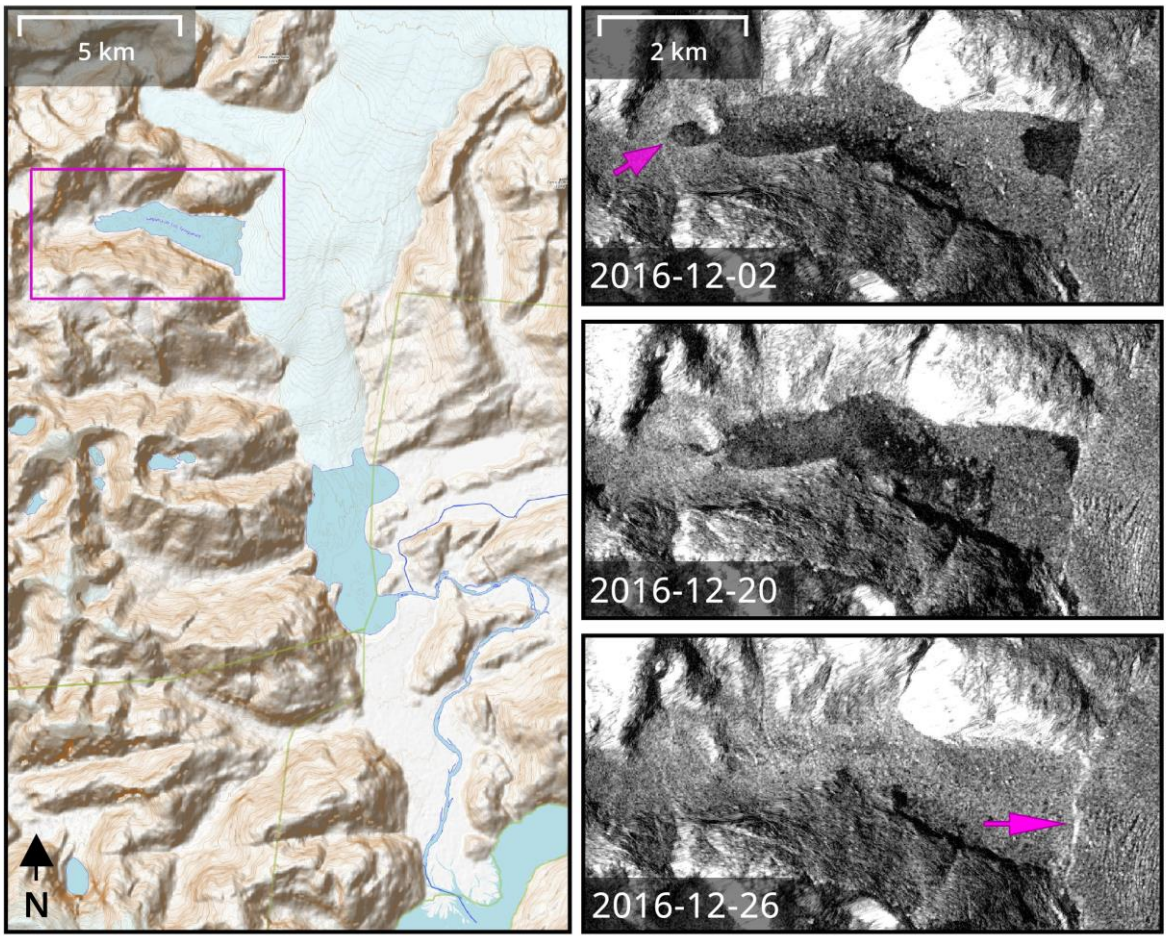

Figure 4.6: Sentinel 1 synthetic aperture radar images of the December 2016 GLOF. Basemap, left, from OpenTopoMap.

Further Sentinel 1 imagery from the 5th and 10th of January 2017 shows the lake already refilling with water, suggesting the conduit opened by the GLOF just days previously had already closed due to ice overburden pressure – figure 4.7. The radar imagery in figure 4.7 was acquired on a descending orbit, so the microwave beam is incident from right to left across the image, and instead of picking up a strong return signal from the exposed ice cliff, the sensor records a "radar shadow". The beam incident angle at the left hand edge of the radar shadow is 39.7 degrees, and the shadow measures ~130 m from the top of the ice cliff to the leftmost edge of the shadow, so the ice cliff rises approximately 100 – 110 m above the lake water level in the 5th January 2017 image.

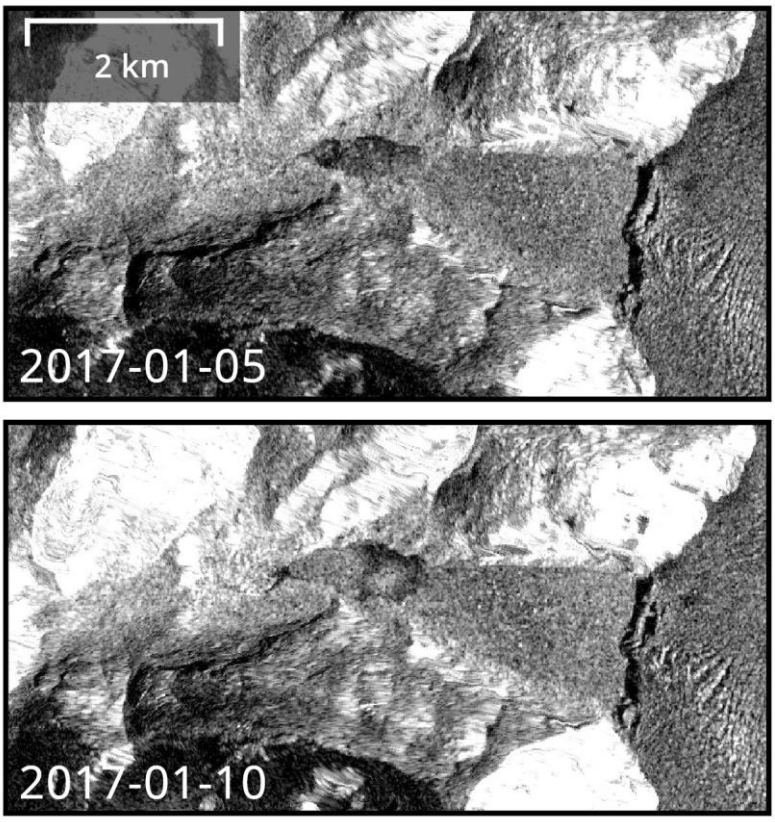

Figure 4.7: Sentinel 1 SAR imagery of the Laguna de los Tempanos beginning to refill with water after the December 2016 GLOF. In these images the ice cliff casts a distinct radar shadow which can be used to estimate its vertical relief at around 100 – 110 m. Note at this point there is already a significant amount of water in the lake, so it is very likely the lake is deeper than 110 m when full.

After the December 2016 event, the next largest GLOF captured in the discharge record happened later in the same summer, between the 27th and 30th of March 2017. Figure 4.8 shows that prior to this GLOF the water level in the Laguna de los Tempanos was lower than the maximum level seen on the 2nd of December in figure 4.6. This might indicate that the partial drainage prior to the December GLOF melted a subaerial channel at the western margin of Steffen Glacier, and effectively lowered the outflow level of the lake. In Sentinel 2 imagery acquired on the 27th of March at 10:28 local time – figure 4.8 panels B and E – icebergs are visibly stranded on dry ground at the lake shoreline, indicating the image was acquired while a GLOF was in progress. This is confirmed by indicating the image acquisition time on the GLOF hydrograph – figure 4.9 – which shows discharge in the Lower Huemules at the point of image acquisition was 826 m^3/s ±25%.

The hydrograph shows that while the March GLOF was smaller – with peak discharge around 900 m^3/s lower than in the December 2016 GLOF, the outburst took around the same amount of time – about 52 hours – and the hydrograph shape is quite similar. The gentle initiation of the rising limb and subsequently exponential rise in discharge is followed by a rapid collapse immediately after peak discharge is reached.

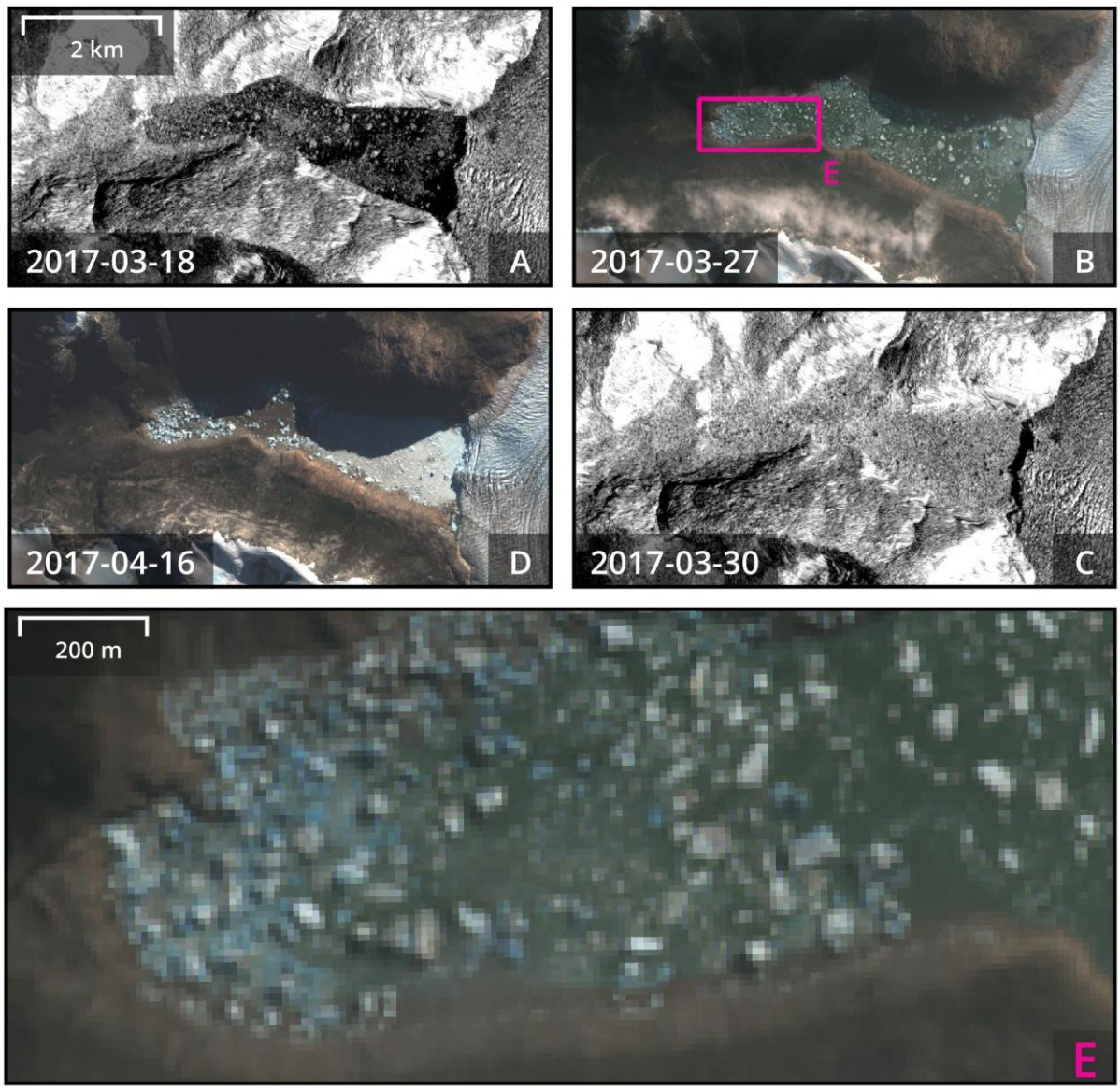

Figure 4.8: Sentinel 1 SAR and Sentinel 2 optical imagery showing the progression of the March 2017 GLOF clockwise from top left through images A, B, C, D. Image B was acquired at 10:28 local time on 2017-03-17, and inset E shows stranded icebergs at the time of acquisition, indicating the GLOF was in progress.

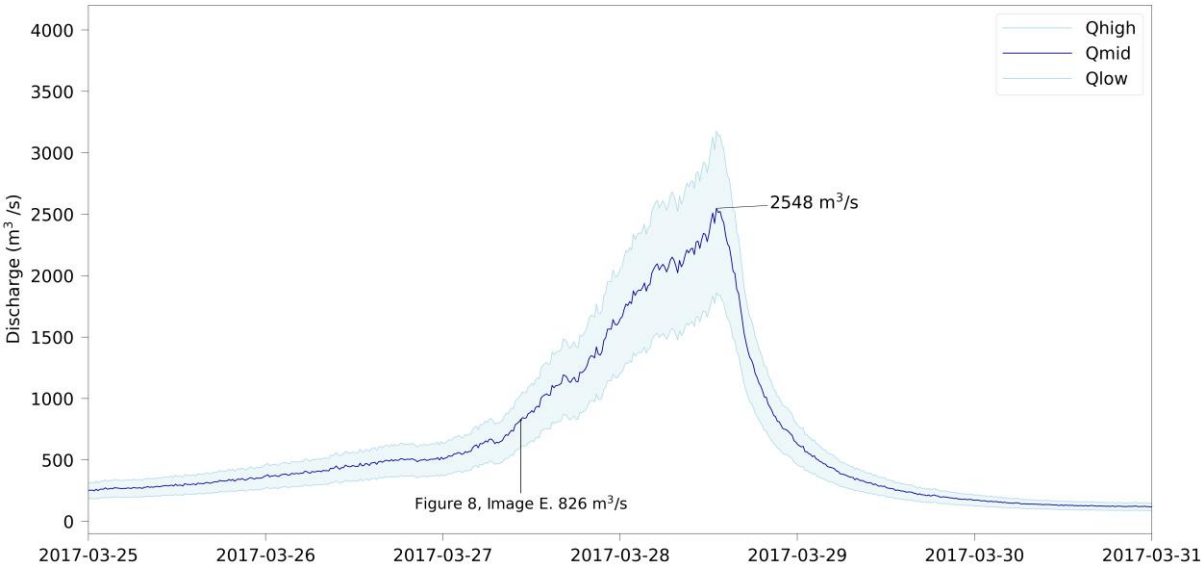

Figure 4.9: GLOF hydrograph of the March 2017 event. Peak discharge was 2548 m^3/s recorded at 2017-03-28 13:04. The acquisition time of the Sentinel 2 image shown in figure 4.8 panels B and E is shown, with a corresponding discharge of 826 m^3/s.

High flow events caused by severe or prolonged precipitation result in a very different hydrograph shape to the GLOF hydrographs shown in figures 4.5 and 4.9. Between the 27th of April and 5th of May 2017, the weather station at Caleta Tortel recorded 249 mm of precipitation. Over the same period the hydrograph from the Lower Huemules River showed a prolonged increase in discharge which peaked at 699 m^3/s ±25%. The hydrograph shape is distinct from confirmed GLOF hydrographs, having a stepped rising limb as discharge responds to changing precipitation, and then a gradual tail indicative of water storage in the catchment – figure 4.10.

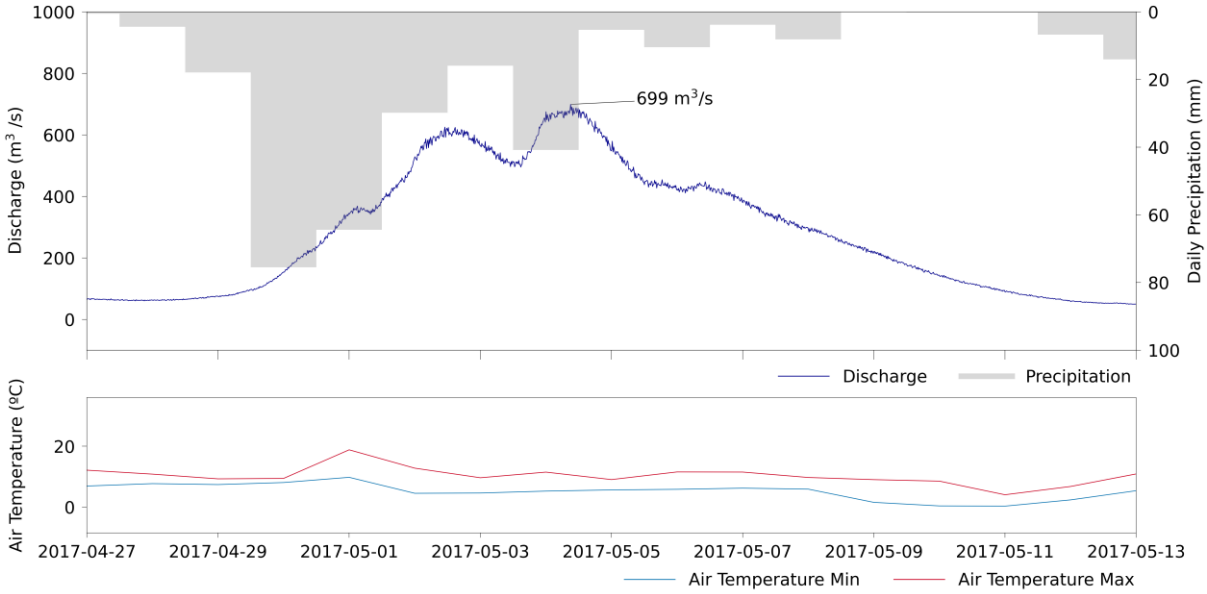

Figure 4.10: A precipitation induced discharge peak from late summer 2017. Note the double peak which corresponds to precipitation recorded at Caleta Tortel, indicating this is an appropriate source of precipitation data for the Huemules catchment in the absence of a closer weather station.

4.1.3 2017 to 2020

Between June 2017 and June 2020, peak discharge did not exceed about 1000 m³/s – figure 4.11. Optical satellite imagery shows the water level Laguna de los Tempanos remains stable throughout this period, and the dense brash ice that previously crowded the lake surface melted away to leave open water, which may indicate reduced iceberg calving from the main trunk of Steffen Glacier.

As previously mentioned, a malfunction of the Hobo pressure transducer in November 2017 resulted in a roughly year long gap in the stage record. This thesis attempts to fill that gap by visually estimating stage from daily Spypoint camera imagery of the river, but the temporal resolution is low, and the stage record is expected to contain around 0.3 m error, which translates to approximately 40 percent of the discharge calculation at 1.3 m stage and 12 percent at 4.3 m stage.

Peak discharge calculated from the Hobo record between 2017 and 2020 was 666 m^3/s on the 24th March 2020, and satellite imagery suggests that glacial lake GL3 drained around this time – figure 4.12. Pansharpened Landsat 8 imagery acquired on the 20th of February 2020 – figure 4.11, image A – shows lake GL3 densely packed with floating ice and no shadow cast by the front of the collapsing glacier to the right of the image centre. On the 8th of April – image B – that glacier front casts a clear shadow over a lakebed scattered with stranded icebergs. This is clear evidence of a GLOF from GL3, but it is not possible to say with certainty whether that event caused the discharge peak recorded on the 24th of March.

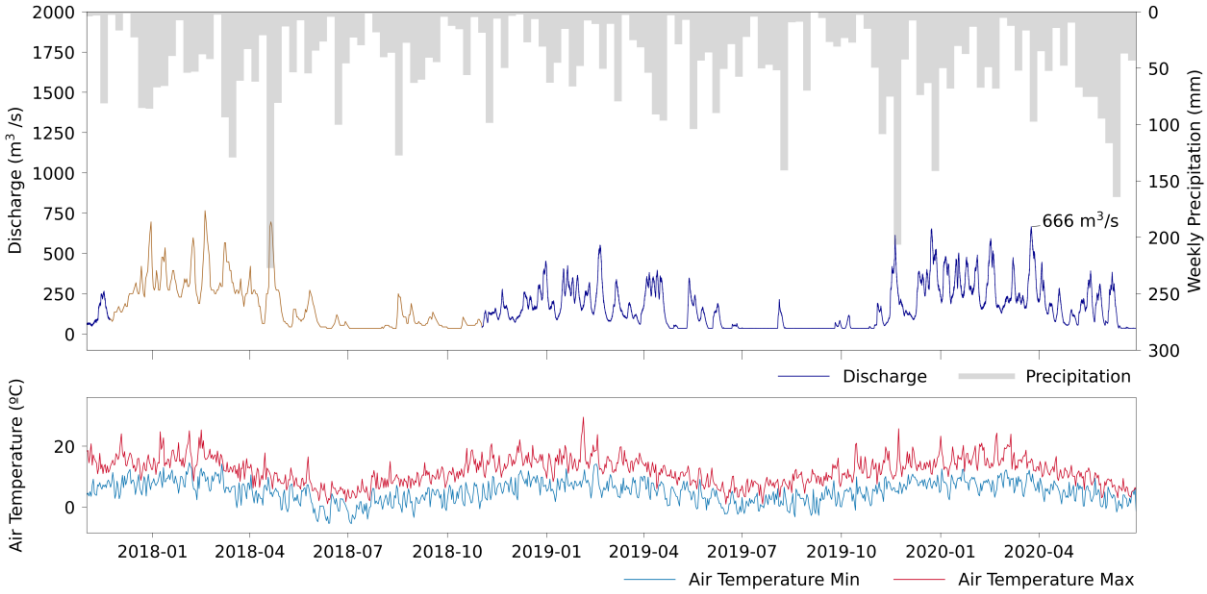

Figure 4.11: Lower Huemules discharge between November 2017 and July 2020.

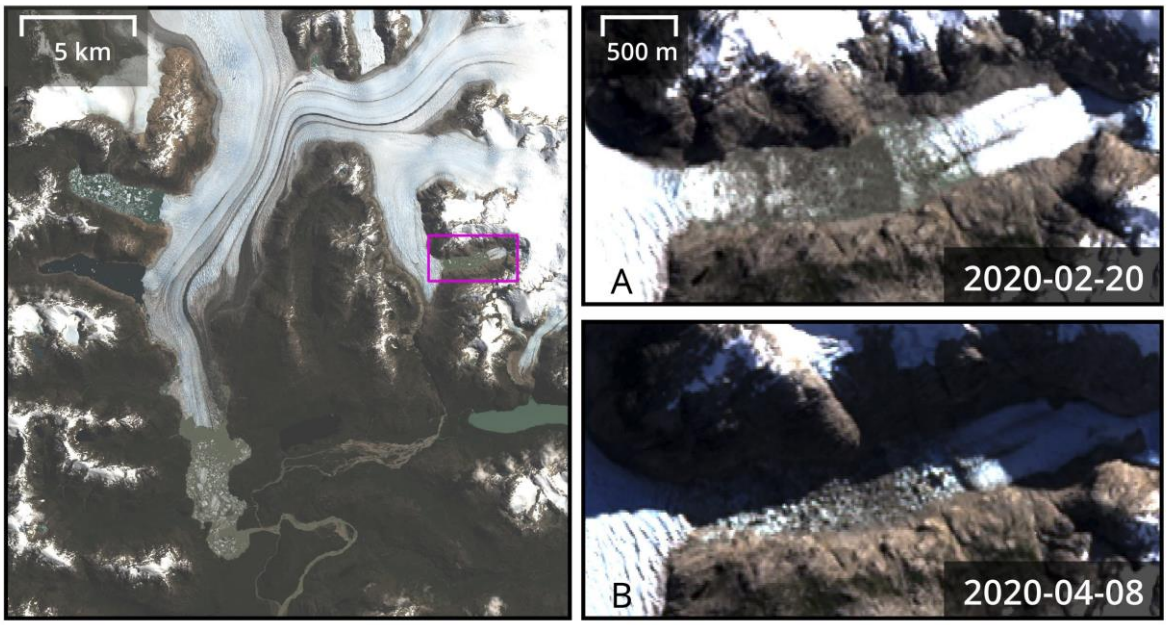

Figure 4.12: Landsat 8 imagery showing the drainage of lake GL3 between the 20th of February 2020 and the 8th of April 2020.

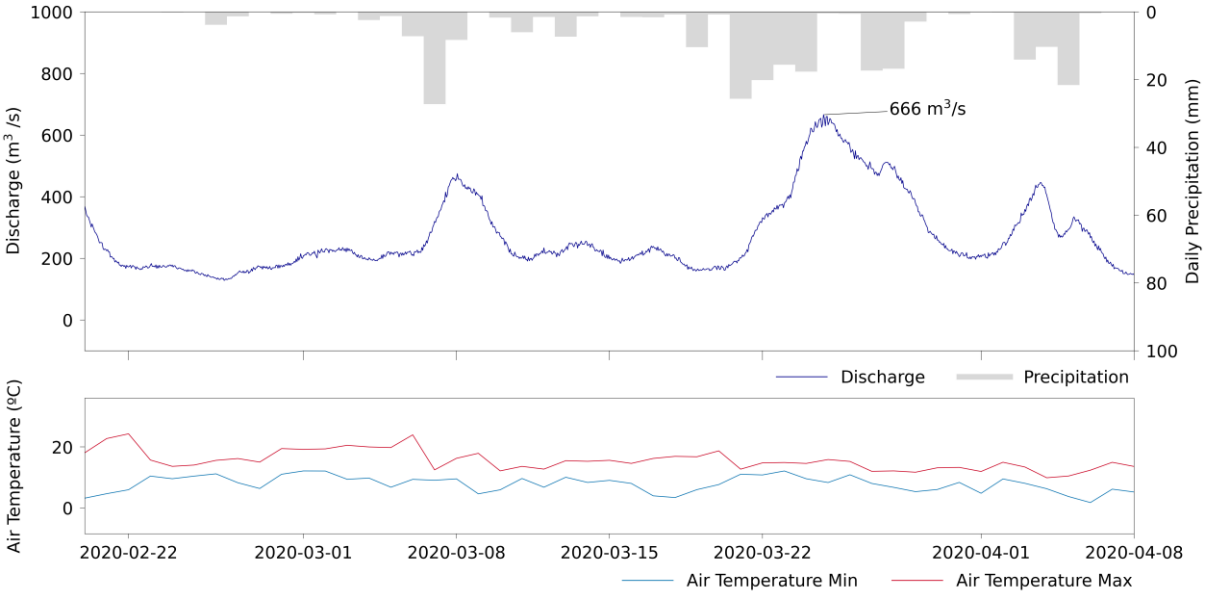

Figure 4.13: Discharge in the Lower Huemules between the 20th of February 2020 and the 8th of April 2020 – the two dates on which Landsat 8 imagery of lake GL3 was acquired showing a GLOF occurred at some point in this period.

4.1.4 2020 to 2022

The two final seasons captured in the discharge record both contain large, satellite confirmed GLOFs with discharge peaks of 1634 m^3/s on the 11th of May 2021 – figure 4.14, and 1058 m^3/s on the 16th of January 2022 – figure 4.15.

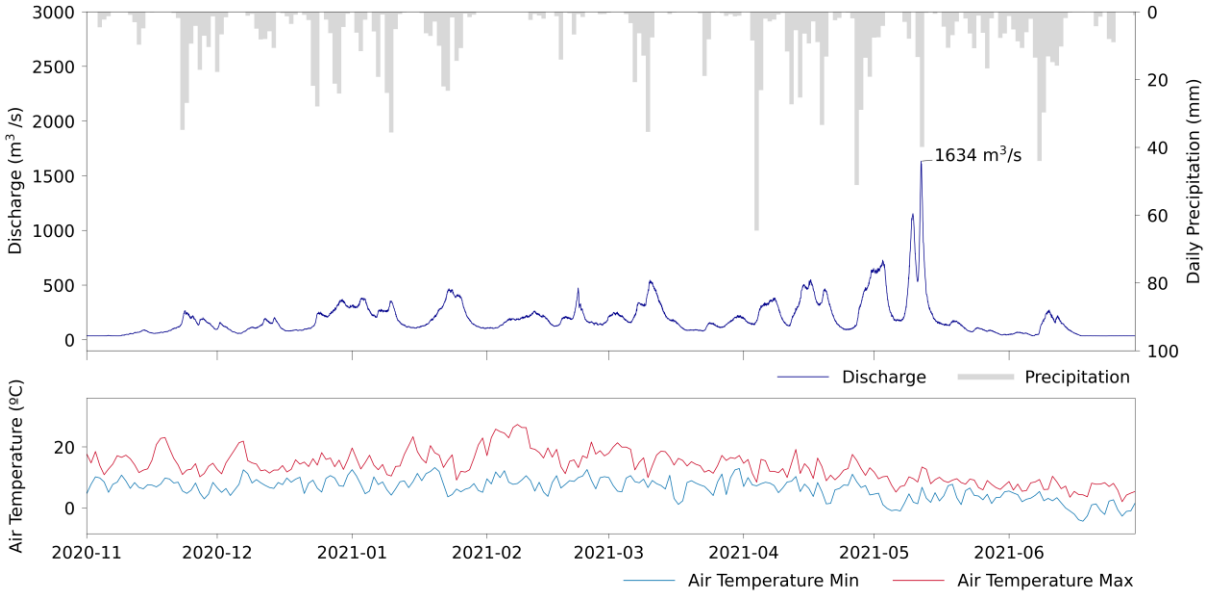

Figure 4.14: Lower Huemules discharge over the 2020 – 2021 Austral summer. The peak discharge of 1634 m^3/s ± 25% was recorded during a partial drainage of the Laguna de los Tempanos on the 11th of May 2021.

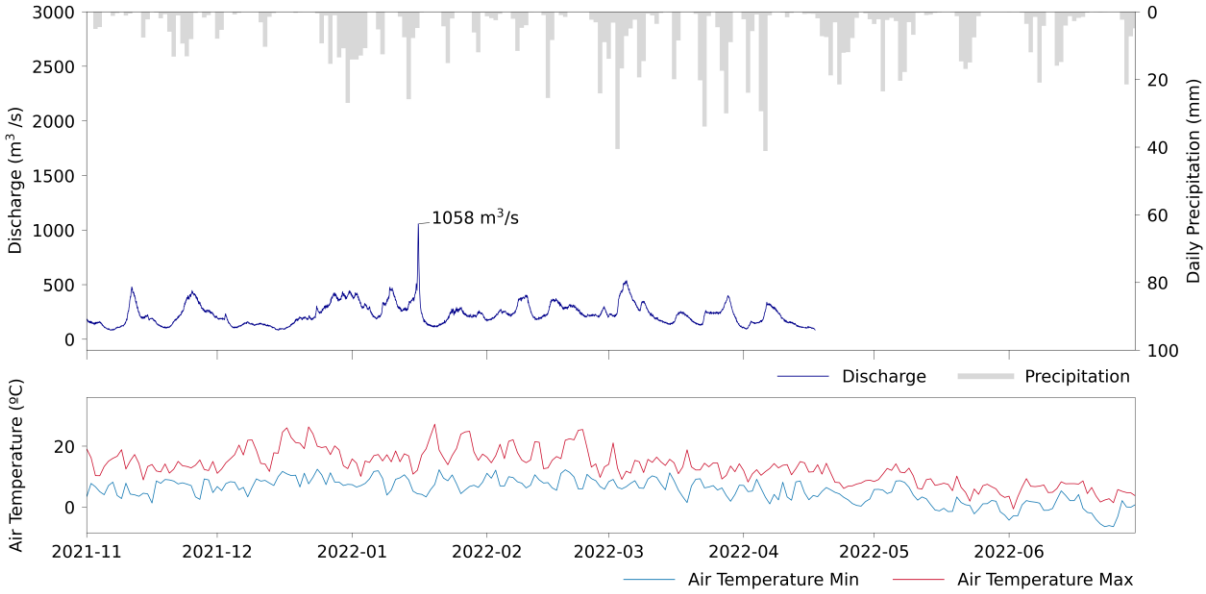

Figure 4.15: Lower Huemules discharge over the 2021 – 2022 Austral summer. The peak discharge of 1058 m^3/s was recorded during a partial drainage of lake GL3 on the 16th of January 2022.

The GLOF recorded on the 11th of May 2021 coincides with a high precipitation event and does not follow the hydrograph shape seen from the 2016 and 2017 GLOFs. The main discharge peak of 1634 $m^3/s \pm 25\%$ is preceded by a smaller peak with discharge around 1100 m^3/s. The rising limb to peak discharge is steeper than the recession limb – figure 4.16, and satellite imagery shows that the Laguna de los Tempanos only partially empties between the 8th and 13th of May – figure 4.17. This indicates the outburst pathway was sub-aerial at the western margin of the glacier where the ice has clearly melted away from the valley wall, rather than the Nye model of sub-glacial drainage in which full emptying of the lake would be expected (Nye, 1976; Spring and Hutter, 1981; Walder and Costa, 1996).

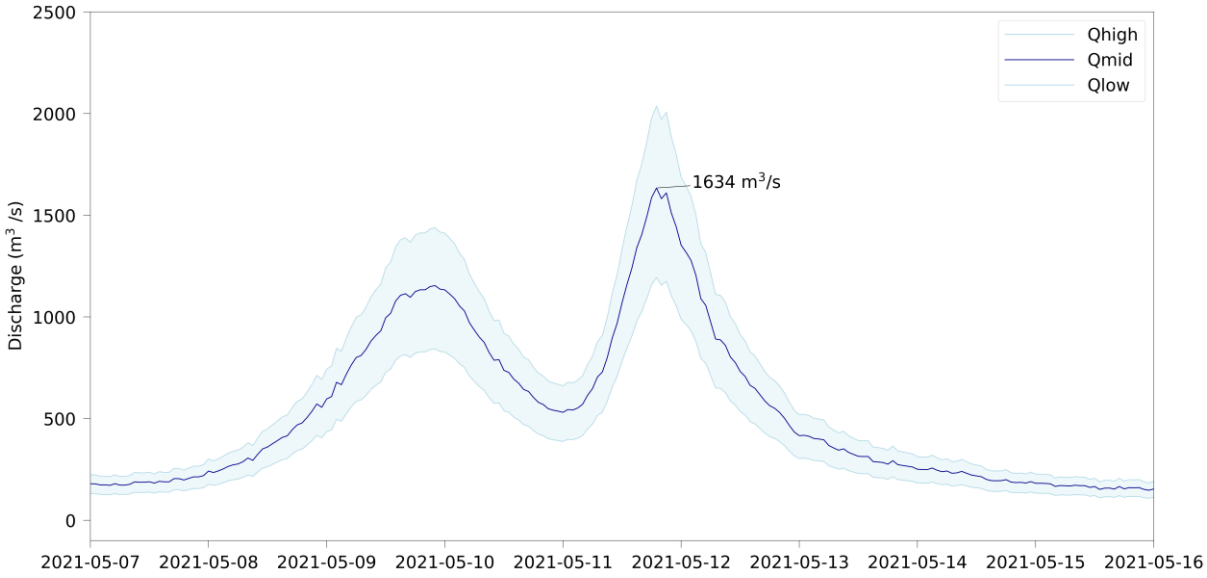

Figure 4.16: Hydrograph of the May 2021 GLOF from the Laguna de los Tempanos. The shallower recession limb of the hydrograph and partial drainage of the lake indicates an ice-marginal sub-aerial pathway rather than the sub-glacial pathways likely during the large GLOFs of 2016 and 2017.

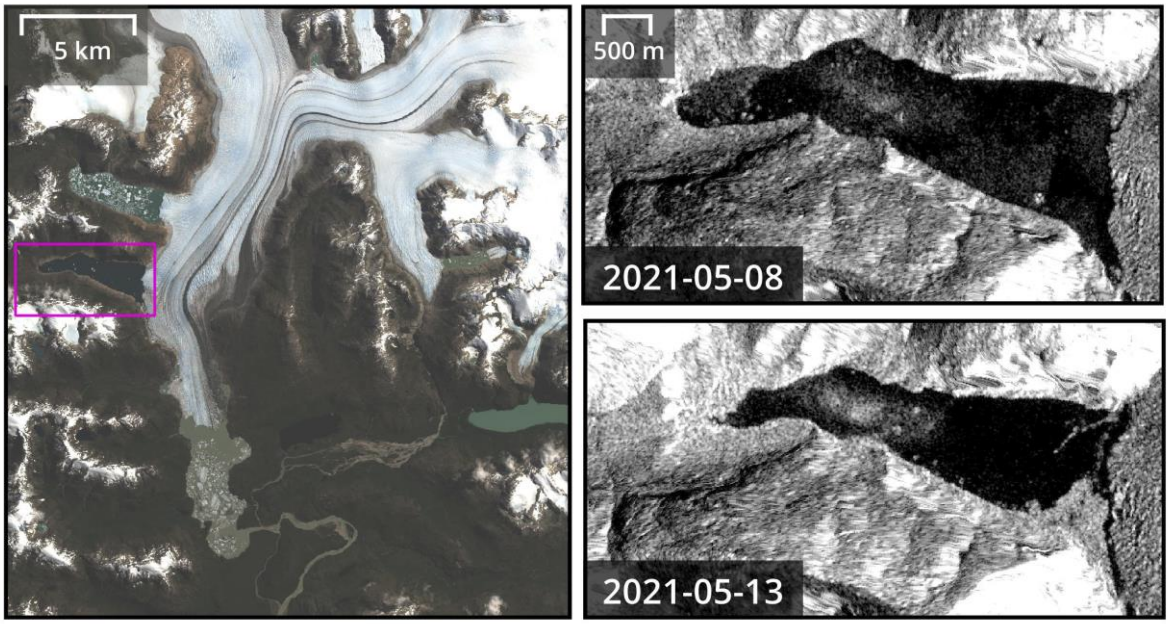

Figure 4.17: Sentinel 1 SAR imagery showing only partial drainage of the Laguna de los Tempanos between the 8th and 13th of May. Note that floating ice next to the ice dam allows the radar shadow to be seen, further confirming a drop in lake level.

The final GLOF captured in the discharge record, on 16th of January 2022, coincides with a drainage of lake GL3 which is visible in both Sentinel 2 optical and Sentinel 1 SAR imagery – figure 4.18. By this date, the glacier that once occupied the valley has retreated 2 km from its junction with glacier HPN4, resulting in a significant increase in the water storage capacity of lake GL3. The GLOF hydrograph – figure 4.19 – again shows peak discharge of 1058 m^3/s ± 25% was reached in around eight to ten hours. The hydrograph has a nearly symmetrical peak, without the sharp recession that typically indicates rapid closure of a sub-glacial drainage conduit, but close examination of the Sentinel 2 imagery in figure 4.18, images A and D, shows no indication that an ice-marginal drainage channel has developed between the ice dam and the tongue of glacier HPN4.

In this case the shallower recession limb is because of the influence of the Upper Huemules floodplain in the drainage path from this source lake. A normalised difference water index image from Sentinel 2 data shows the January 2022 GLOF caused avulsion of the Upper Huemules river channel – figure 4.20.

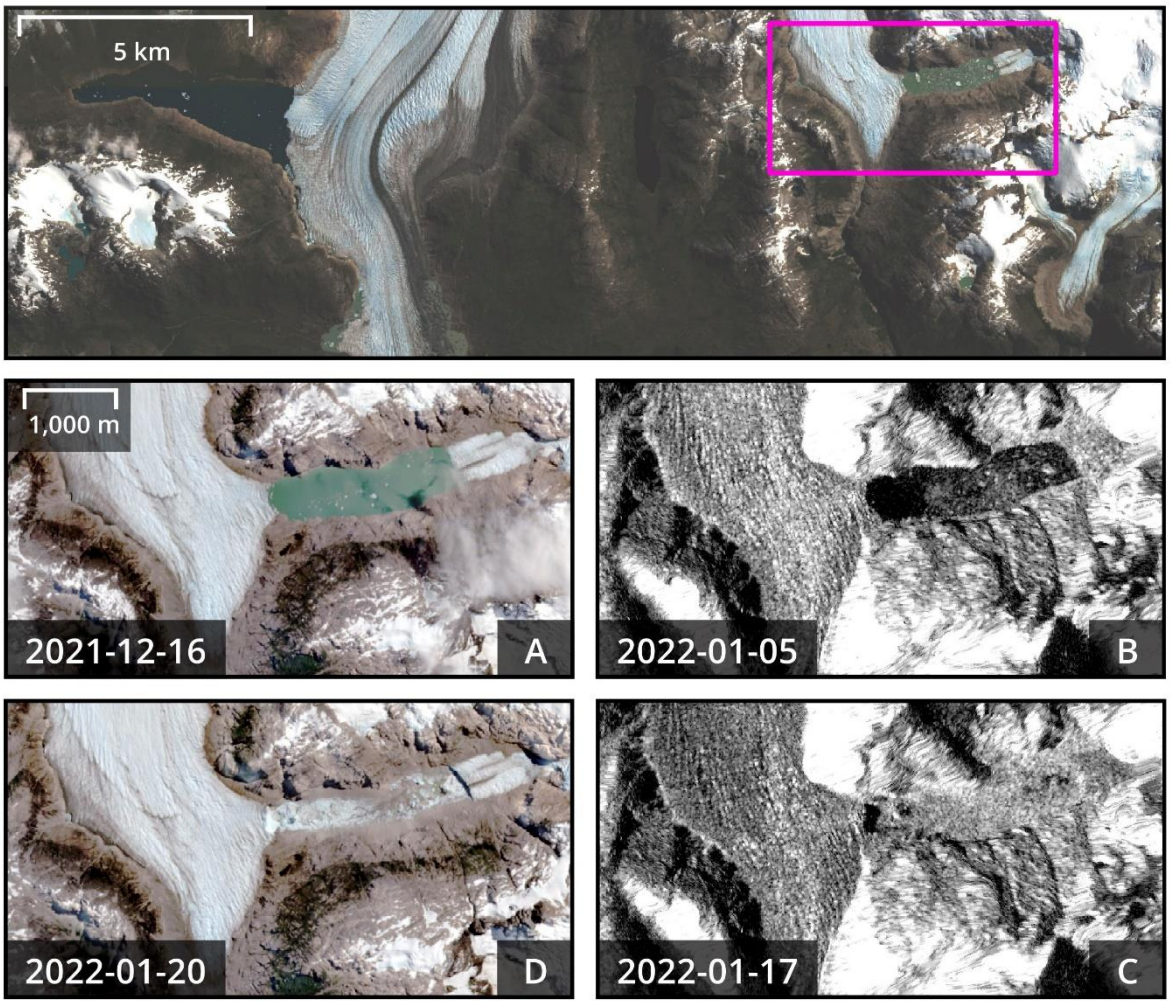

Figure 4.18: Satellite imagery showing the outburst flood from lake GL3 in January 2022.

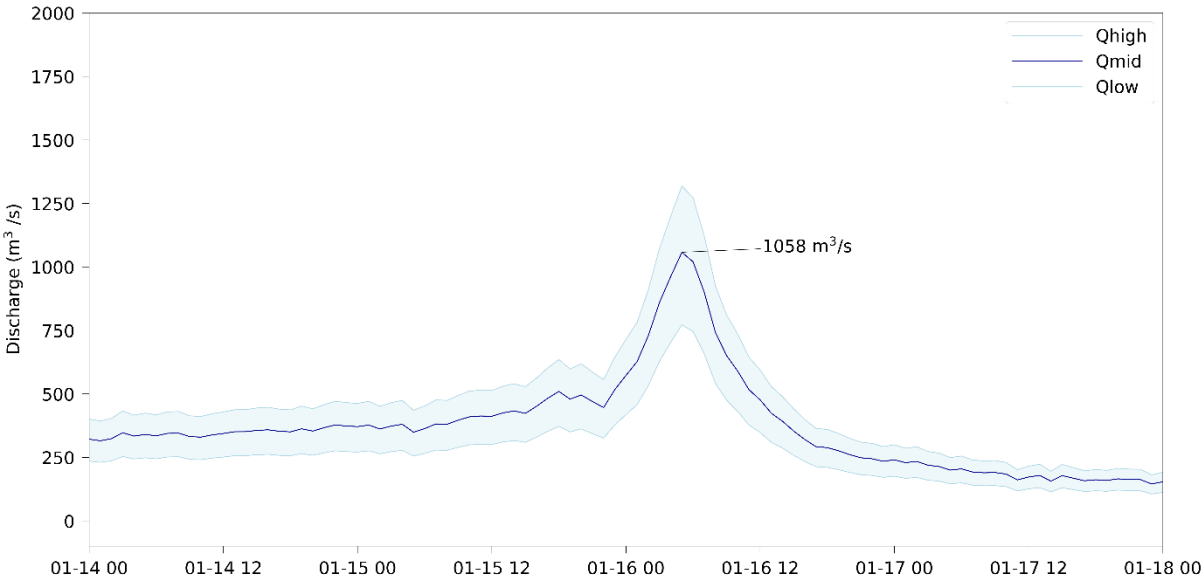

Figure 4.19: Hydrograph of the January 2022 outburst flood from lake GL3.

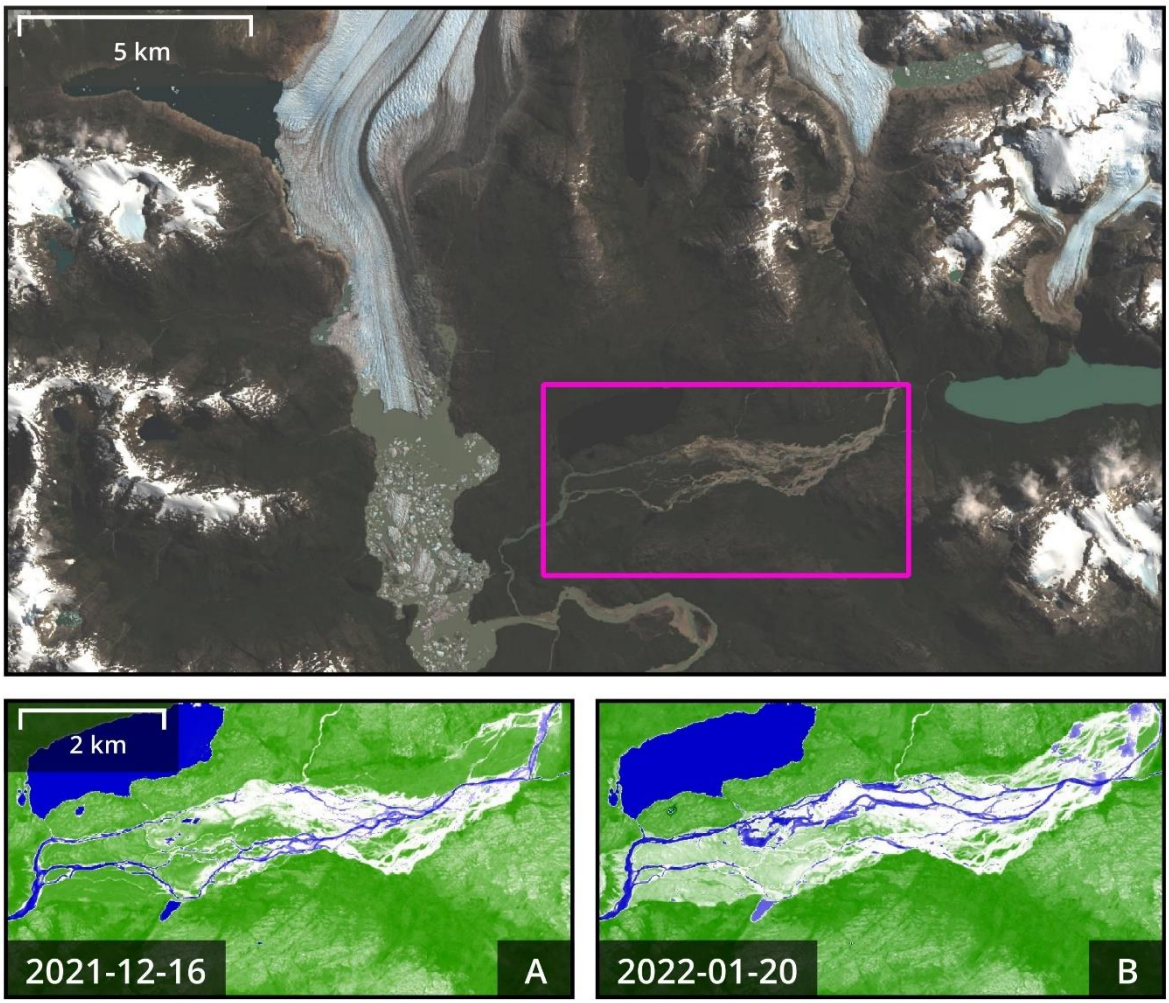

Figure 4.20: Sentinel 2 normalised difference water index showing the floodplain of the Upper Huemules river before and after the January 2022 GLOF from lake GL3.

4.2 Outburst flood volumes from the Laguna de los Tempanos

As described in section 3.4 on rating corroboration, the volume of the Laguna de los Tempanos was calculated as 0.254 km^3 prior to the December 2016 GLOF, and 0.211 km^3 prior to the March 2017 GLOF using satellite derived measurements of lake surface area and empirical scaling relationships (Loriaux and Casassa, 2013). By calculating the area under the GLOF hydrographs and subtracting base flow — figure 4.21 — the volume of excess water discharged during the GLOFs can be found and used as a further test of the envelope rating — table 4.2.

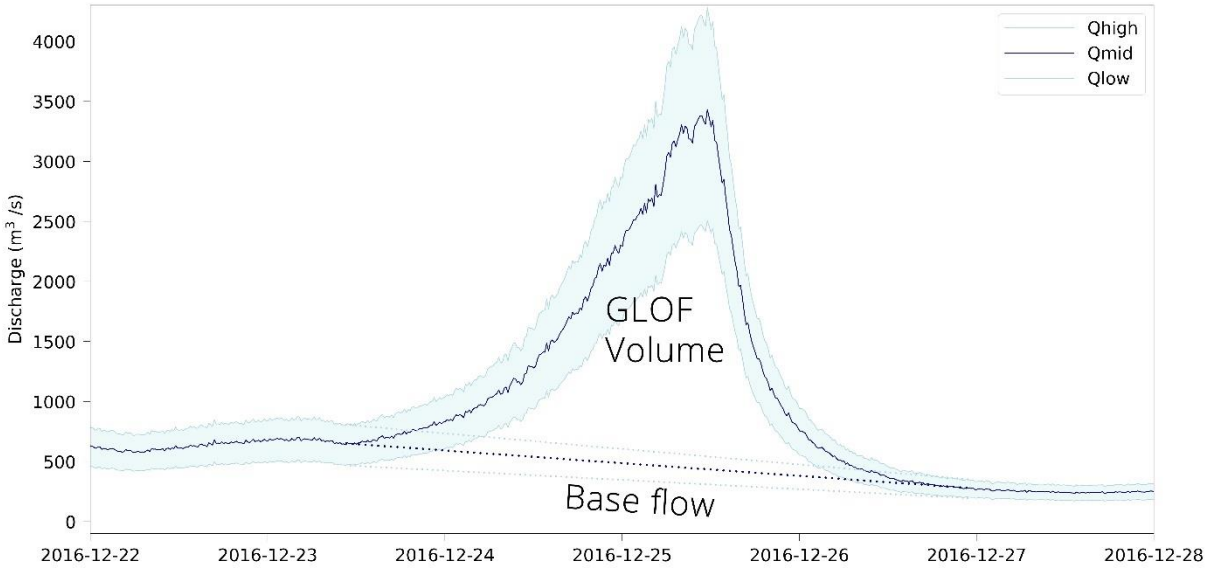

Figure 4.21: Illustration of GLOF volume calculation from the hydrograph.

Table 4.2: GLOF volumes (V_{min}, V_{best}, V_{max}) calculated from the hydrographs compared to estimates for source lake volume made using the surface area to volume relationship (Loriaux and Casassa, 2013) (V scalar). All volumes are expressed in km^3.

	V_{min}	V_{best}	V_{max}	V scalar
December 2016	0.18	0.25	0.36	0.25
March 2017	0.14	0.19	0.23	0.21

The volume comparison presented here shows that 'excess GLOF volume' calculated from the hydrograph of the best estimate (Q_{best}) rating is very close to the source lake volume calculated using the scaling relationship between lake surface area and volume that has previously been used to calculate glacial lake volumes in the Northern Patagonian Icefield (Loriaux and Casassa, 2013).

In combination with max Q corroboration from the Clague—Matthews relationship (section 3.4), and the close fit to gauged discharge at low stage, these results indicate that in the absence of more precise direct measurement, this rating can be considered an acceptable

description of the stage—discharge relationship in the Lower Huemules River for the whole range of in-bank flows assuming the morphology of the bedrock reach remains stable.

4.3 Glacial retreat and future GLOF cycles

As mass loss and frontal retreat of Steffen and HPN4 glaciers is expected to continue, and possibly accelerate over the coming decades (Abdel Jaber et al., 2019; Bravo et al., 2021; Dussaillant et al., 2018; Jaber et al., 2014), future GLOF hazard in the Steffen—Huemules will enter a new phase as the Laguna de los Tempanos becomes further connected to Steffen Lake by a stable drainage network, and lake GL1 or "No Name Lake" enters a GLOF cycle which may involve full volume outbursts for the first time (Aniya et al., 2020). Measurements of lake GL1 made from satellite imagery acquired during November 2022 indicate the lake volume is 0.21 km^3, so while GLOF magnitude from the Laguna de los Tempanos has declined since 2016, GL1 can be expected to flood with outburst discharges of around 2500 ± 625 m^3/s if it enters a full GLOF cycle at this volume.

Indeed, recent imagery from the Sentinel 1 SAR satellite suggests the Laguna de los Tempanos might already be in the final stages of its GLOF phase. Since its last partial GLOF drainage between the 19th and 31st of December 2022, the lake area has remained stable at around 1.8 km^2 — less than half its previous surface area.

5 Conclusions and directions for further research

The primary aim of this project was to test whether remote sensing and hydraulic principles could be used to improve the rating for the Huemules River. Testing the envelope rating, firstly by estimates of max GLOF discharge derived from source lake volume and the Clague—Matthews relationship, and second by GLOF volume calculated from the hydrograph, suggests that the rating presented in section 3.3 is suitable for defining the in-bank stage—discharge relationship in the Lower Huemules in the absence of a more accurate and comprehensive survey of the river. To our knowledge the rating and discharge record presented in this thesis is the first from a directly gauged glacial river draining the Northern Patagonian Icefield and is therefore a useful step towards refining knowledge of catchment scale water balance and mass loss from Steffen Glacier, as well as contributing to improved understanding of the sea level rise contribution of the Northern Patagonian Icefield (Pellicciotti et al., 2014; Van Wyk de Vries et al., 2023).

Second, the shape of the hydrographs from December 2016 and March 2017 suggests that outburst floods from the Laguna de los Tempanos drained subglacially. The rising limb of the hydrographs shows an almost exponential rise in discharge to the flood peak before a rapid collapse. This type of GLOF hydrograph has been described for many ice-dammed lake outburst floods, and fits the physical models for subglacial drainage that were discovered by Röthlisberger (1972), Nye (1976), Fowler and Ng (1996) and others. As Steffen Glacier has continued to retreat, subsequent GLOFs from the Laguna de los Tempanos indicate a change in the drainage system. The GLOF in May 2021 was overall a much lower magnitude event with a more gradual recession limb, and satellite imagery before and after the event indicate the lake only partially drained. This may indicate a development of the subaerial drainage channel at the western margin of the glacier and would have implications for sediment transport during GLOFs. While the source lake is in a GLOF phase determined by high magnitude subglacial drainage events, more sediment may be eroded from the lakebed and subglacial till during the outburst. As the lake level drops and subaerial drainage becomes dominant there is likely to be a reduction in sediment transport during outburst floods which will have knock on effects on downstream river channel morphology

and fjord ecosystems. Fjord biogeochemical cycles in particular are very sensitive to sediment and nutrient inputs from glacial rivers, so quantifying those inputs provides an improved foundation for further research into these aquatic critical zones (Bianchi et al., 2020).

The GLOF from lake GL3 in January 2022 is difficult to define by its hydrograph because of the buffering effect of the Upper Huemules floodplain. Satellite imagery shows GL3 has increased in size over the last four years, and the lack of a well-developed subaerial drainage pathway indicate GL3 might drain subglacially under the snout of HPN4. As HPN4 retreats and GL3 transitions out of its GLOF phase into a stable drainage regime, the GLOF triggered avulsions of the Upper Huemules River may reduce or cease completely.

The magnitude of GLOF events and the timing of lakes transitioning into and out of GLOF cycles has important implications for risk management in the floodplain and delta areas of the Lower Huemules. This study shows that GLOF volume and peak discharge from outbursts of the Laguna de los Tempanos (LdlT) has declined since 2016, and recent satellite imagery shows its transition out of a GLOF phase is well advanced. Lake GL1, just to the north of the LdlT, currently holds roughly the same volume of water as the LdlT did in 2016/2017 and is likely to enter a full volume GLOF cycle in the future as Steffen Glacier continues to retreat. The complexity of subglacial drainage and GLOF triggers make it impossible to predict when this cycle will begin, but when it does GL1 has the potential to cause GLOFs with peak discharge up to around 4000 m^3/s. Communicating this information to at risk families living near the Huemules flood path should be a priority, if it has not already been done.

The discharge record in the Lower Huemules over the period between August 2016 and April 2022 shows the same seasonal cycle as other glacially fed rivers of the Northern Patagonian Icefield. Discharge is dominated by melt induced high flows between December and March and much lower flow during the June to November winter period is punctuated by precipitation induced peaks that can exceed mean summer discharge. GLOFs have only been recorded between December and May, indicating the possibility of a temperature

based trigger – whether due to seasonal ice velocity changes or glacial lake warming. Both the mean annual peak discharge of around 650 m^3/s ± 25%, and the December 2016 GLOF peak discharge of 3432 m^3/s ± 25% are lower than the equivalent values reported for the Colonia River and Cachet 2 GLOFs (Jacquet et al., 2017), but the lack of a gauging station and rating for the Colonia River itself shows the need for greater monitoring of the glacial rivers draining the NPI.

Until this rating is improved by a comprehensive channel survey and installation of a long-term, remotely monitored gauging station in the Huemules River, it can be used as a basis for further research on the Steffen—Huemules system and the Baker—Martinez fjords. Particularly interesting areas for research where this rating may be useful include quantifying inputs of freshwater, sediment and dissolved organic matter to Steffen Fjord, and investigating potential links between ice-dammed lake GLOF cycles and glacial ice dynamics.

6 References

Abdel Jaber, W., Rott, H., Floricioiu, D., Wuite, J., Miranda, N., 2019. Heterogeneous spatial and temporal pattern of surface elevation change and mass balance of the Patagonian ice fields between 2000 and 2016. The Cryosphere 13, 2511–2535. https://doi.org/10.5194/tc-13-2511-2019

Aggarwal, S., Rai, S.C., Thakur, P.K., Emmer, A., 2017a. Inventory and recently increasing GLOF susceptibility of glacial lakes in Sikkim, Eastern Himalaya. Geomorphology 295, 39–54. https://doi.org/10.1016/j.geomorph.2017.06.014

Aggarwal, S., Rai, S.C., Thakur, P.K., Emmer, A., 2017b. Inventory and recently increasing GLOF susceptibility of glacial lakes in Sikkim, Eastern Himalaya. Geomorphology 295, 39–54. https://doi.org/10.1016/j.geomorph.2017.06.014

Amann, B., Bertrand, S., Alvarez-Garreton, C., Reid, B., 2022. Seasonal Variations in Fjord Sediment Grain Size: A Pre-requisite for Hydrological and Climate Reconstructions in Partially Glacierized Watersheds (Baker River, Patagonia). Journal of Geophysical Research: Earth Surface 127, e2021JF006391. https://doi.org/10.1029/2021JF006391

Anacona, P.I., Mackintosh, A., Norton, K., 2015. Reconstruction of a glacial lake outburst flood (GLOF) in the Engaño Valley, Chilean Patagonia: Lessons for GLOF risk management. Science of The Total Environment 527–528, 1–11. https://doi.org/10.1016/j.scitotenv.2015.04.096

Aniya, M., 2013. Holocene glaciations of Hielo Patagónico (Patagonia Icefield), South America: A brief review. Geochemical Journal 47, 97–105. https://doi.org/10.2343/geochemj.1.0171

Aniya, M., Casassa, G., 1998. Variations of Patagonian glaciers, South America, utilizing RADARSAT images.

Aniya, M., Dusaillant, A., O'Kuinghttons, J., Barcaza, G., Bravo, S., 2020. GLOFs of Laguna de los Témpanos, glacier-dammed side lake of Glaciar Steffen, Hielo Patagónico Norte, Chile, since 1974. Bulletin of Glacier Research 38, 13–24. https://doi.org/10.5331/bgr.20R01

Baker, V.R., Benito, G., Rudoy, A.N., 1993. Paleohydrology of Late Pleistocene Superflooding, Altay Mountains, Siberia. Science 259, 348–350. https://doi.org/10.1126/science.259.5093.348

Banerjee, I., McDonald, B.C., 1975. Nature of Esker Sedimentation.

Benito, G., Thorndycraft, V.R., 2020. Catastrophic glacial-lake outburst flooding of the Patagonian Ice Sheet. Earth-Science Reviews 200, 102996. https://doi.org/10.1016/j.earscirev.2019.102996

Benito, G., Thorndycraft, V.R., Medialdea, A., Machado, M.J., Sancho, C., Dussaillant, A., 2021. Declining discharge of glacier outburst floods through the Holocene in central Patagonia. Quaternary Science Reviews 256, 106810. https://doi.org/10.1016/j.quascirev.2021.106810

Benn, D., Gulley, J., Luckman, A., Adamek, A., Glowacki, P.S., 2009. Englacial drainage systems formed by hydrologically driven crevasse propagation. Journal of Glaciology 55, 513–523. https://doi.org/10.3189/002214309788816669

Bianchi, T.S., Arndt, S., Austin, W.E.N., Benn, D.I., Bertrand, S., Cui, X., Faust, J.C., Koziorowska-Makuch, K., Moy, C.M., Savage, C., Smeaton, C., Smith, R.W., Syvitski, J., 2020. Fjords as Aquatic Critical Zones (ACZs). Earth-Science Reviews 203, 103145. https://doi.org/10.1016/j.earscirev.2020.103145

Birgand, F., Lellouche, G., Appelboom, T.W., 2013. Measuring flow in non-ideal conditions for short-term projects: Uncertainties associated with the use of stage-discharge rating curves. Journal of Hydrology 503, 186–195. https://doi.org/10.1016/j.jhydrol.2013.09.007

Boulton, G.S., Hagdorn, M., Maillot, P.B., Zatsepin, S., 2009. Drainage beneath ice sheets: groundwater–channel coupling, and the origin of esker systems from former ice sheets. Quaternary Science Reviews, Quaternary Glaciodynamics 28, 621–638. https://doi.org/10.1016/j.quascirev.2008.05.009

Bräuning, A., 2006. Tree-ring evidence of 'Little Ice Age' glacier advances in southern Tibet. The Holocene 16, 369–380. https://doi.org/10.1191/0959683606hl922rp

Bravo, C., Bozkurt, D., Ross, A.N., Quincey, D.J., 2021. Projected increases in surface melt and ice loss for the Northern and Southern Patagonian Icefields. Sci Rep 11, 16847. https://doi.org/10.1038/s41598-021-95725-w

Burke, M.J., Brennand, T.A., Perkins, A.J., 2012. Transient subglacial hydrology of a thin ice sheet: insights from the Chasm esker, British Columbia, Canada. Quaternary Science Reviews 58, 30–55. https://doi.org/10.1016/j.quascirev.2012.09.004

Carrivick, J.L., Tweed, F.S., 2013. Proglacial lakes: character, behaviour and geological importance. Quaternary Science Reviews 78, 34–52. https://doi.org/10.1016/j.quascirev.2013.07.028

Clague, J.J., Mathews, W.H., 1973. The Magnitude of Jökulhlaups. Journal of Glaciology 12, 501–504. https://doi.org/10.3189/S0022143000031907

Clarke, G.K.C., 2003. Hydraulics of subglacial outburst floods: new insights from the Spring–Hutter formulation. Journal of Glaciology 49, 299–313. https://doi.org/10.3189/172756503781830728

Clarke, G.K.C., 1982. Glacier Outburst Floods From "Hazard Lake", Yukon Territory, and the Problem of Flood Magnitude Prediction. Journal of Glaciology 28, 3–21. https://doi.org/10.3189/S0022143000011746

Cook, S.J., Quincey, D.J., 2015. Estimating the volume of Alpine glacial lakes. Earth Surf. Dynam. 3, 559–575. https://doi.org/10.5194/esurf-3-559-2015

Dabiri, Z., Hölbling, D., Abad, L., Guðmundsson, S., 2021. Comparing the Applicability of Sentinel-1 and Sentinel-2 for Mapping the Evolution of Ice-marginal Lakes in Southeast Iceland. giforum 1, 46–52. https://doi.org/10.1553/giscience2021_01_s46

Dai, K., Wen, N., Fan, X., Deng, J., Zhang, L., Liang, R., Liu, J., Xu, Q., 2022. Seasonal Changes of Glacier Lakes in Tibetan Plateau Revealed by Multipolarization SAR Data. IEEE Geoscience and Remote Sensing Letters 19, 1–5. https://doi.org/10.1109/LGRS.2021.3131717

Davies, B.J., Glasser, N.F., 2012. Accelerating shrinkage of Patagonian glaciers from the Little Ice Age (~AD 1870) to 2011. J. Glaciol. 58, 1063–1084. https://doi.org/10.3189/2012JoG12J026

Dussaillant, A., Benito, G., Buytaert, W., Carling, P., Meier, C., Espinoza, F., 2010. Repeated glacial-lake outburst floods in Patagonia: an increasing hazard? Nat Hazards 54, 469–481. https://doi.org/10.1007/s11069-009-9479-8

Dussaillant, I., Berthier, E., Brun, F., 2018. Geodetic Mass Balance of the Northern Patagonian Icefield from 2000 to 2012 Using Two Independent Methods. Front. Earth Sci. 6, 8. https://doi.org/10.3389/feart.2018.00008

Dussaillant J., A., Buytaert, W., Meier, C., Espinoza, F., 2012. Hydrological regime of remote catchments with extreme gradients under accelerated change: the Baker basin in Patagonia. Hydrological Sciences Journal 57, 1530–1542. https://doi.org/10.1080/02626667.2012.726993

Elbert, J., Grosjean, M., von Gunten, L., Urrutia, R., Fischer, D., Wartenburger, R., Ariztegui, D., Fujak, M., Hamann, Y., 2012. Quantitative high-resolution winter (JJA) precipitation reconstruction from varved sediments of Lago Plomo 47°S, Patagonian

Andes, ad 1530–2002. The Holocene 22, 465–474. https://doi.org/10.1177/0959683611425547

Emmer, A., Allen, S.K., Carey, M., Frey, H., Huggel, C., Korup, O., Mergili, M., Sattar, A., Veh, G., Chen, T.Y., Cook, S.J., Correas-Gonzalez, M., Das, S., Diaz Moreno, A., Drenkhan, F., Fischer, M., Immerzeel, W.W., Izagirre, E., Joshi, R.C., Kougkoulos, I., Kuyakanon Knapp, R., Li, D., Majeed, U., Matti, S., Moulton, H., Nick, F., Piroton, V., Rashid, I., Reza, M., Ribeiro de Figueiredo, A., Riveros, C., Shrestha, F., Shrestha, M., Steiner, J., Walker-Crawford, N., Wood, J.L., Yde, J.C., 2022. Progress and challenges in glacial lake outburst flood research (2017–2021): a research community perspective. Natural Hazards and Earth System Sciences 22, 3041–3061. https://doi.org/10.5194/nhess-22-3041-2022

Emmer, A., Harrison, S., Mergili, M., Allen, S., Frey, H., Huggel, C., 2020. 70 years of lake evolution and glacial lake outburst floods in the Cordillera Blanca (Peru) and implications for the future. Geomorphology 365, 107178. https://doi.org/10.1016/j.geomorph.2020.107178

Espizua, L.E., Pitte, P., 2009. The Little Ice Age glacier advance in the Central Andes (35°S), Argentina. Palaeogeography, Palaeoclimatology, Palaeoecology, Long-term multi-proxy climate reconstructions and dynamics in South America (LOTRED-SA): State of the art and perspectives 281, 345–350. https://doi.org/10.1016/j.palaeo.2008.10.032

Foresta, L., Gourmelen, N., Weissgerber, F., Nienow, P., Williams, J.J., Shepherd, A., Drinkwater, M.R., Plummer, S., 2018. Heterogeneous and rapid ice loss over the Patagonian Ice Fields revealed by CryoSat-2 swath radar altimetry. Remote Sensing of Environment 211, 441–455. https://doi.org/10.1016/j.rse.2018.03.041

Fowler, A.C., Ng, F.S.L., 1996. The role of sediment transport in the mechanics of jökulhlaups. Annals of Glaciology 22, 255–259. https://doi.org/10.3189/1996AoG22-1-255-259

Frey, H., 2017. Glacier Lake Outburst Floods, in: Richardson, D., Castree, N., Goodchild, M.F., Kobayashi, A., Liu, W., Marston, R.A. (Eds.), International Encyclopedia of Geography: People, the Earth, Environment and Technology. John Wiley & Sons, Ltd, Oxford, UK, pp. 1–5. https://doi.org/10.1002/9781118786352.wbieg0665

Frey, H., Huggel, C., Bühler, Y., Buis, D., Burga, M.D., Choquevilca, W., Fernandez, F., García Hernández, J., Giráldez, C., Loarte, E., Masias, P., Portocarrero, C., Vicuña, L., Walser, M., 2016. A robust debris-flow and GLOF risk management strategy for a data-scarce catchment in Santa Teresa, Peru. Landslides 13, 1493–1507. https://doi.org/10.1007/s10346-015-0669-z

Glasser, N.F., Jansson, K.N., Harrison, S., Kleman, J., 2008. The glacial geomorphology and Pleistocene history of South America between 38°S and 56°S. Quaternary Science Reviews 27, 365–390. https://doi.org/10.1016/j.quascirev.2007.11.011

Glen, J.W., 1954. The Stability of Ice-Dammed Lakes and other Water-Filled Holes in Glaciers. Journal of Glaciology 2, 316–318. https://doi.org/10.3189/S0022143000025132

Gulley, J.D., Benn, D.I., Screaton, E., Martin, J., 2009. Mechanisms of englacial conduit formation and their implications for subglacial recharge. Quaternary Science Reviews 28, 1984–1999. https://doi.org/10.1016/j.quascirev.2009.04.002

Haeberli, W., Kääb, A., Mühll, D.V., Teysseire, P., 2001. Prevention of outburst floods from periglacial lakes at Grubengletscher, Valais, Swiss Alps. Journal of Glaciology 47, 111–122. https://doi.org/10.3189/172756501781832575

Herschy, R., 1993. The velocity-area method. Flow Measurement and Instrumentation, Special Issue - Open Channel Measurements 4, 7–10. https://doi.org/10.1016/0955-5986(93)90004-3

Hock, R., Rasul, G., Adler, C., Cáceres, B., Gruber, S., Hirabayashi, Y., Jackson, M., Kääb, A., Kang, S., Kutuzov, S., 2019. High mountain areas, in: IPCC Special Report on the Ocean and Cryosphere in a Changing Climate. H.-O. Pörtner, DC Roberts, V. Masson-Delmotte, P. Zhai, M. Tignor, E …, pp. 131–202.

Holmes, R., 2016. River rating complexity. Presented at the Proceedings River Flow Conference; Taylor & Francis Group: St. Louis, MO, USA.

Huggel, C., Kääb, A., Haeberli, W., Teysseire, P., Paul, F., 2002. Remote sensing based assessment of hazards from glacier lake outbursts: a case study in the Swiss Alps. Can. Geotech. J. 39, 316–330. https://doi.org/10.1139/t01-099

Iribarren Anacona, P., Norton, K., Mackintosh, A., Escobar, F., Allen, S., Mazzorana, B., Schaefer, M., 2018. Dynamics of an outburst flood originating from a small and high-altitude glacier in the Arid Andes of Chile. Nat Hazards 94, 93–119. https://doi.org/10.1007/s11069-018-3376-y

Jaber, W.A., Floricioiu, D., Rott, H., 2014. Glacier dynamics of the Northern Patagonia Icefield derived from SRTM, TanDEM-X and TerraSAR-X data, in: 2014 IEEE Geoscience and Remote Sensing Symposium. Presented at the IGARSS 2014 - 2014 IEEE International Geoscience and Remote Sensing Symposium, IEEE, Quebec City, QC, pp. 4018–4021. https://doi.org/10.1109/IGARSS.2014.6947367

Jacquet, J., McCoy, S.W., McGrath, D., Nimick, D.A., Fahey, M., O'kuinghttons, J., Friesen, B.A., Leidich, J., 2017. Hydrologic and geomorphic changes resulting from episodic

glacial lake outburst floods: Rio Colonia, Patagonia, Chile: CHANGE RESULTING FROM RIO COLONIA GLOFS. Geophys. Res. Lett. 44, 854–864. https://doi.org/10.1002/2016GL071374

Jakob, L., Gourmelen, N., 2023. Glacier Mass Loss Between 2010 and 2020 Dominated by Atmospheric Forcing. Geophysical Research Letters 50, e2023GL102954. https://doi.org/10.1029/2023GL102954

Jansson, K.N., 2003. Early Holocene glacial lakes and ice marginal retreat pattern in Labrador/Ungava, Canada. Palaeogeography, Palaeoclimatology, Palaeoecology 193, 473–501. https://doi.org/10.1016/S0031-0182(03)00262-1

Kiang, J.E., Gazoorian, C., McMillan, H., Coxon, G., Le Coz, J., Westerberg, I.K., Belleville, A., Sevrez, D., Sikorska, A.E., Petersen-Øverleir, A., Reitan, T., Freer, J., Renard, B., Mansanarez, V., Mason, R., 2018. A Comparison of Methods for Streamflow Uncertainty Estimation. Water Resources Research 54, 7149–7176. https://doi.org/10.1029/2018WR022708

Kilpatrick, A., Cobb, E.D., 1985. Measurement of Discharge using Tracers, in: Techniques of Water-Resources Investigations. U.S. Geological Survey, pp. 2–7.

Kjær, K.H., Bjørk, A.A., Kjeldsen, K.K., Hansen, E.S., Andresen, C.S., Siggaard-Andersen, M.-L., Khan, S.A., Søndergaard, A.S., Colgan, W., Schomacker, A., Woodroffe, S., Funder, S., Rouillard, A., Jensen, J.F., Larsen, N.K., 2022. Glacier response to the Little Ice Age during the Neoglacial cooling in Greenland. Earth-Science Reviews 227, 103984. https://doi.org/10.1016/j.earscirev.2022.103984

Koch, J., Kilian, R., 2005. 'Little Ice Age' glacier fluctuations, Gran Campo Nevado, southernmost Chile. The Holocene 15, 20–28. https://doi.org/10.1191/0959683605hl780rp

Korup, O., 2012. Earth's portfolio of extreme sediment transport events. Earth-Science Reviews 112, 115–125. https://doi.org/10.1016/j.earscirev.2012.02.006

Li, J., Sheng, Y., 2012. An automated scheme for glacial lake dynamics mapping using Landsat imagery and digital elevation models: a case study in the Himalayas. International Journal of Remote Sensing 33, 5194–5213. https://doi.org/10.1080/01431161.2012.657370

Liestøl, O., 1956. Glacier dammed lakes in Norway.

Loriaux, T., Casassa, G., 2013. Evolution of glacial lakes from the Northern Patagonia Icefield and terrestrial water storage in a sea-level rise context. Global and Planetary Change 102, 8. http://dx.doi.org/10.1016/j.gloplacha.2012.12.012

Lützow, N., Veh, G., Korup, O., 2023. A global database of historic glacier lake outburst floods. Earth System Science Data Discussions 1–27. https://doi.org/10.5194/essd-2022-449

Marshall, M., 2020. Assessing the impact of glacier retreat on organic matter export and cycling in Chilean Patagonia (PhD). University of Bristol, Bristol, UK.

Marshall, M.G., Kellerman, A.M., Wadham, J.L., Hawkings, J.R., Daneri, G., Torres, R., Pryer, H.V., Beaton, A., Ng, H.C., Urra, A., Robinson, L.F., Spencer, R.G.M., 2021. Seasonal Changes in Dissolved Organic Matter Composition in a Patagonian Fjord Affected by Glacier Melt Inputs. Frontiers in Marine Science 8, 276. https://doi.org/10.3389/fmars.2021.612386

McCammon, I., 2002. Evidence of heuristic traps in recreational avalanche accidents. International Snow Science Workshop.

McMillan, H., Krueger, T., Freer, J., 2012. Benchmarking observational uncertainties for hydrology: rainfall, river discharge and water quality. Hydrological Processes 26, 4078–4111. https://doi.org/10.1002/hyp.9384

Meerhoff, E., Castro, L., Tapia, F., 2013. Influence of freshwater discharges and tides on the abundance and distribution of larval and juvenile Munida gregaria in the Baker river estuary, Chilean Patagonia. Continental Shelf Research 61–62, 1–11. https://doi.org/10.1016/j.csr.2013.04.025

Meerhoff, E., Castro, L.R., Tapia, F.J., Pérez-Santos, I., 2019. Hydrographic and Biological Impacts of a Glacial Lake Outburst Flood (GLOF) in a Patagonian Fjord. Estuaries and Coasts 42, 132–143. https://doi.org/10.1007/s12237-018-0449-9

Meier, W.J.-H., Grießinger, J., Hochreuther, P., Braun, M.H., 2018. An Updated Multi-Temporal Glacier Inventory for the Patagonian Andes With Changes Between the Little Ice Age and 2016. Frontiers in Earth Science 6.

Motschmann, A., Huggel, C., Muñoz, R., Thür, A., 2020. Towards integrated assessments of water risks in deglaciating mountain areas: water scarcity and GLOF risk in the Peruvian Andes. Geoenviron Disasters 7, 26. https://doi.org/10.1186/s40677-020-00159-7

Murton, D.K., Murton, J.B., 2012. Middle and Late Pleistocene glacial lakes of lowland Britain and the southern North Sea Basin. Quaternary International, Commemorative Volume in Honour of Jim Teller 260, 115–142. https://doi.org/10.1016/j.quaint.2011.07.034

Ng, F., Björnsson, H., 2003. On the Clague–Mathews relation for jökulhlaups. Journal of Glaciology 49, 161–172. https://doi.org/10.3189/172756503781830836

Nye, J.F., 1976. Water Flow in Glaciers: Jökulhlaups, Tunnels and Veins. Journal of Glaciology 17, 181–207. https://doi.org/10.3189/S002214300001354X

O'Connor, J.E., Baker, V.R., 1992. Magnitudes and implications of peak discharges from glacial Lake Missoula. GSA Bulletin 104, 267–279. https://doi.org/10.1130/0016-7606(1992)104<0267:MAIOPD>2.3.CO;2

O'Connor, J.E., Costa, J.E., 2004. The World's Largest Floods, Past and Present.

Osti, R., Egashira, S., 2009. Hydrodynamic characteristics of the Tam Pokhari glacial lake outburst flood in the Mt. Everest region, Nepal. Hydrological Processes 23, 2943–2955. https://doi.org/10.1002/hyp.7405

O'Sullivan, P.E., 1983. Annually-laminated lake sediments and the study of Quaternary environmental changes — a review. Quaternary Science Reviews 1, 245–313. https://doi.org/10.1016/0277-3791(83)90008-2

Pellicciotti, F., Ragettli, S., Carenzo, M., McPhee, J., 2014. Changes of glaciers in the Andes of Chile and priorities for future work. Science of The Total Environment 493, 1197–1210. https://doi.org/10.1016/j.scitotenv.2013.10.055

Pereira, A., Cornero, C., Matos, A.C.O.C., Pacino, M.C., Blitzkow, D., Pereira, A., Cornero, C., Matos, A.C.O.C., Pacino, M.C., Blitzkow, D., 2021. Detection of total water mass changes in the Patagonian glaciers area by satellite gravimetry. Geofísica internacional 60, 161–174. https://doi.org/10.22201/igeof.00167169p.2021.60.2.2086

Piret, L., Bertrand, S., Hawkings, J., Kylander, M.E., Torrejón, F., Amann, B., Wadham, J., 2021. High-resolution fjord sediment record of a receding glacier with growing intermediate proglacial lake (Steffen Fjord, Chilean Patagonia). Earth Surface Processes and Landforms 46, 239–251. https://doi.org/10.1002/esp.5015

Piret, L., Bertrand, S., Nguyen, N., Hawkings, J., Rodrigo, C., Wadham, J., 2022. Long-lasting impacts of a 20th century glacial lake outburst flood on a Patagonian fjord-river system (Pascua River). Geomorphology 399, 108080. https://doi.org/10.1016/j.geomorph.2021.108080

Povilitis, A., 1986. Huemuls in Areas Adjacent to Glaciers in Southern Chile. Mountain Research and Development 6, 273–275. https://doi.org/10.2307/3673397

Richter, A., Groh, A., Horwath, M., Ivins, E., Marderwald, E., Hormaechea, J.L., Perdomo, R., Dietrich, R., 2019. The Rapid and Steady Mass Loss of the Patagonian Icefields

throughout the GRACE Era: 2002–2017. Remote Sensing 11, 909. https://doi.org/10.3390/rs11080909

Richter, E., 1892. Urkunden über die Ausbrüche des Vernagt- und Gurglergletschers im 17. und 18. Jahrhundert. Engelhorn.

Rignot, E., Rivera, A., Casassa, G., 2003. Contribution of the Patagonia Icefields of South America to Sea Level Rise. Science 302, 434–437. https://doi.org/10.1126/science.1087393

Rivera, A., Benham, T., Casassa, G., Bamber, J., Dowdeswell, J.A., 2007. Ice elevation and areal changes of glaciers from the Northern Patagonia Icefield, Chile. Global and Planetary Change 59, 126–137. https://doi.org/10.1016/j.gloplacha.2006.11.037

Röthlisberger, H., 1972. Water Pressure in Intra- and Subglacial Channels. Journal of Glaciology 11, 177–203. https://doi.org/10.3189/S0022143000022188

Rowan, A.V., 2017. The 'Little Ice Age' in the Himalaya: A review of glacier advance driven by Northern Hemisphere temperature change. The Holocene 27, 292–308. https://doi.org/10.1177/0959683616658530

Shugar, D.H., Burr, A., Haritashya, U.K., Kargel, J.S., Watson, C.S., Kennedy, M.C., Bevington, A.R., Betts, R.A., Harrison, S., Strattman, K., 2020. Rapid worldwide growth of glacial lakes since 1990. Nature Climate Change 1–7. https://doi.org/10.1038/s41558-020-0855-4

Spring, U., Hutter, K., 1981. Numerical studies of Jökulhlaups. Cold Regions Science and Technology 4, 227–244. https://doi.org/10.1016/0165-232X(81)90006-9

Stotter, M., 1846. Die Gletscher des Vernagtthales in Tirol und ihre Geschichte. Wagner.

Strozzi, T., Wiesmann, A., Kääb, A., Joshi, S., Mool, P., 2012. Glacial lake mapping with very high resolution satellite SAR data. Nat. Hazards Earth Syst. Sci. 12, 2487–2498. https://doi.org/10.5194/nhess-12-2487-2012

Syvitski, J.P.M., 1989. On the deposition of sediment within glacier-influenced fjords: Oceanographic controls. Marine Geology 85, 301–329. https://doi.org/10.1016/0025-3227(89)90158-8

Taylor, C., Robinson, T.R., Dunning, S., Rachel Carr, J., Westoby, M., 2023. Glacial lake outburst floods threaten millions globally. Nat Commun 14, 487. https://doi.org/10.1038/s41467-023-36033-x

Thorarinsson, S., 1939. Chapter IX. The ice dammed lakes of Iceland with particular reference to their values as indicators of glacier oscillations. Geografiska Annaler 21, 216–242. https://doi.org/10.1080/20014422.1939.11880679

van der Veen, C.J., 1998. Fracture mechanics approach to penetration of surface crevasses on glaciers. Cold Regions Science and Technology 27, 31–47. https://doi.org/10.1016/S0165-232X(97)00022-0

Van Wyk de Vries, M., Ito, E., Shapley, M., Brignone, G., Romero, M., Wickert, A.D., Miller, L.H., MacGregor, K.R., 2022. Physical Limnology and Sediment Dynamics of Lago Argentino, the World's Largest Ice-Contact Lake. Journal of Geophysical Research: Earth Surface 127, e2022JF006598. https://doi.org/10.1029/2022JF006598

Van Wyk de Vries, M., Romero, M., Penprase, S.B., Ng, G.-H.C., Wickert, A.D., 2023. Increasing rate of 21st century volume loss of the Patagonian Icefields measured from proglacial river discharge. Journal of Glaciology 1–16. https://doi.org/10.1017/jog.2023.9

Vandekerkhove, E., Bertrand, S., Crescenzi Lanna, E., Reid, B., Pantoja, S., 2020a. Modern sedimentary processes at the heads of Martínez Channel and Steffen Fjord, Chilean Patagonia. Marine Geology 419, 106076. https://doi.org/10.1016/j.margeo.2019.106076

Vandekerkhove, E., Bertrand, S., Mauquoy, D., McWethy, D., Reid, B., Stammen, S., Saunders, K.M., Torrejón, F., 2020b. Neoglacial increase in high-magnitude glacial lake outburst flood frequency, upper Baker River, Chilean Patagonia (47°S). Quaternary Science Reviews 248, 106572. https://doi.org/10.1016/j.quascirev.2020.106572

Veh, G., Lützow, N., Kharlamova, V., Petrakov, D., Hugonnet, R., Korup, O., 2022. Trends, Breaks, and Biases in the Frequency of Reported Glacier Lake Outburst Floods. Earth's Future 10, e2021EF002426. https://doi.org/10.1029/2021EF002426

Wagener, T., Gleeson, T., Coxon, G., Hartmann, A., Howden, N., Pianosi, F., Rahman, M., Rosolem, R., Stein, L., Woods, R., 2021. On doing hydrology with dragons: Realizing the value of perceptual models and knowledge accumulation. WIREs Water 8, e1550. https://doi.org/10.1002/wat2.1550

Walder, J.S., Costa, J.E., 1996. Outburst Floods from Glacier-Dammed Lakes: The Effect of Mode of Lake Drainage on Flood Magnitude. Earth Surface Processes and Landforms 21, 701–723. https://doi.org/10.1002/(SICI)1096-9837(199608)21:8<701::AID-ESP615>3.0.CO;2-2

Wang, X., Guo, X., Yang, C., Liu, Q., Wei, J., Zhang, Yong, Liu, S., Zhang, Yanlin, Jiang, Z., Tang, Z., 2020. Glacial lake inventory of high-mountain Asia in 1990 and 2018

derived from Landsat images. Earth System Science Data 12, 2169–2182. https://doi.org/10.5194/essd-12-2169-2020

Wangchuk, S., Bolch, T., Robson, B.A., 2022. Monitoring glacial lake outburst flood susceptibility using Sentinel-1 SAR data, Google Earth Engine, and persistent scatterer interferometry. Remote Sensing of Environment 271, 112910. https://doi.org/10.1016/j.rse.2022.112910

Wangchuk, S., Bolch, T., Zawadzki, J., 2019. Towards automated mapping and monitoring of potentially dangerous glacial lakes in Bhutan Himalaya using Sentinel-1 Synthetic Aperture Radar data. International Journal of Remote Sensing 40, 4642–4667. https://doi.org/10.1080/01431161.2019.1569789

Warren, C.R., Sugden, D.E., 1993. The Patagonian Icefields: A Glaciological Review. Arctic and Alpine Research 25, 316–331. https://doi.org/10.1080/00040851.1993.12003018

Wilson, R., Glasser, N.F., Reynolds, J.M., Harrison, S., Anacona, P.I., Schaefer, M., Shannon, S., 2018. Glacial lakes of the Central and Patagonian Andes. Global and Planetary Change 162, 275–291. https://doi.org/10.1016/j.gloplacha.2018.01.004

World Meteorological Organization (WMO), 2010. Manual on Stream Gauging, Vol. I: Fieldwork, WMO. WMO, Geneva.

Zavala, C., Arcuri, M., Di Meglio, M., Zorzano, A., Otharán, G., Irastorza, A., Torresi, A., 2021. Deltas: a new classification expanding Bates's concepts. Journal of Palaeogeography 10, 23. https://doi.org/10.1186/s42501-021-00098-w

Zhang, M., Chen, F., Tian, B., Liang, D., Yang, A., 2019. High-frequency glacial lake mapping using time series of Sentinel-1A/1B SAR imagery: An assessment for southeastern TibetanPlateau. Nat. Hazards Earth Syst. Sci. Discuss. 1–18. https://doi.org/10.5194/nhess-2019-219

Zolitschka, B., Francus, P., Ojala, A.E.K., Schimmelmann, A., 2015. Varves in lake sediments – a review. Quaternary Science Reviews 117, 1–41. https://doi.org/10.1016/j.quascirev.2015.03.019